Journal of Computational Neuroscience 15, 367–389, 2003

AHP's, HAP's and DAP's: How Potassium Currents Regulate the Excitability of Rat Supraoptic Neurones

PETER ROPER
National Institute of Diabetes and Digestive and Kidney Diseases, National Institutes of Health, Bethesda, MD 20892, USA
pete.roper@nih.gov

JOSEPH CALLAWAY, TALENT SHEVCHENKO, RYOICHI TERUYAMA AND WILLIAM ARMSTRONG
Department of Anatomy and Neurobiology, University of Tennessee College of Medicine, 855 Monroe Avenue, Memphis, TN 38163, USA

Received March 10, 2003; Revised August 20, 2003; Accepted August 22, 2003

Action Editor: John Rinzel

Abstract. We have constructed mathematical models of the electrical activity of two hypothalamic supraoptic neuro-secretory cell-types, and we support our models with new calcium imaging and in vitro electrophysiological data. These cells are neurones that project to the pituitary gland and secrete either of two hormones, oxytocin or vasopressin, into the blood from their axonal terminals. Oxytocin-secreting and vasopressin-secreting cells are closely related and physically they differ only subtly, however when physiologically stressed their discharge patterns are dramatically distinct. We first show how each potassium current contributes to the action-potentials and after-potentials observed in these cells, and we show how these after-potentials are correlated to intra-cellular calcium elevations. We then show how these currents regulate the excitability of these cells and consequently shape their discharge pattern.

1. Introduction

Oxytocin (OT) and arginine vasopressin (AVP) magnocellular neurosecretory cells (MNC's) in the rat hypothalamus are the best described peptidergic neurones in the mammalian brain. They project to the neurohypophysis, and when electrically stimulated their terminals secrete either OT or AVP directly into the blood *via* exocytosis. Release is primarily a response to: osmotic stress (AVP and OT); haemorrhage (AVP and OT); parturition (OT); and suckling (OT), and is a function of both firing rate and of the discharge pattern. OT and AVP cells are morphologically and electrically very similar and their action potentials cannot easily be distinguished. Spikes from both cell types are sterotypic with a fast rise and a repolarization that briefly overshoots the rest potential.

After spiking the membrane potential evinces several after-potentials before relaxing to the rest potential. First the repolarizing overshoot merges into an evanescent hyperpolarized after-potential (HAP^1) (see Fig. 1a), which has a slower decay than the passive response of the membrane and so is actively sustained by a conductance (Andrew and Dudek, 1984b; Bourque et al., 1985). A substantial fraction of MNC's then express a slow depolarizing overshoot that follows the initial HAP (Andrew and Dudek, 1983) (see Fig. 1c). This depolarizing after-potential (DAP) is both calcium- and voltage-dependent (Bourque, 1986; Andrew, 1987; Li et al., 1995), and is more frequently expressed in AVP

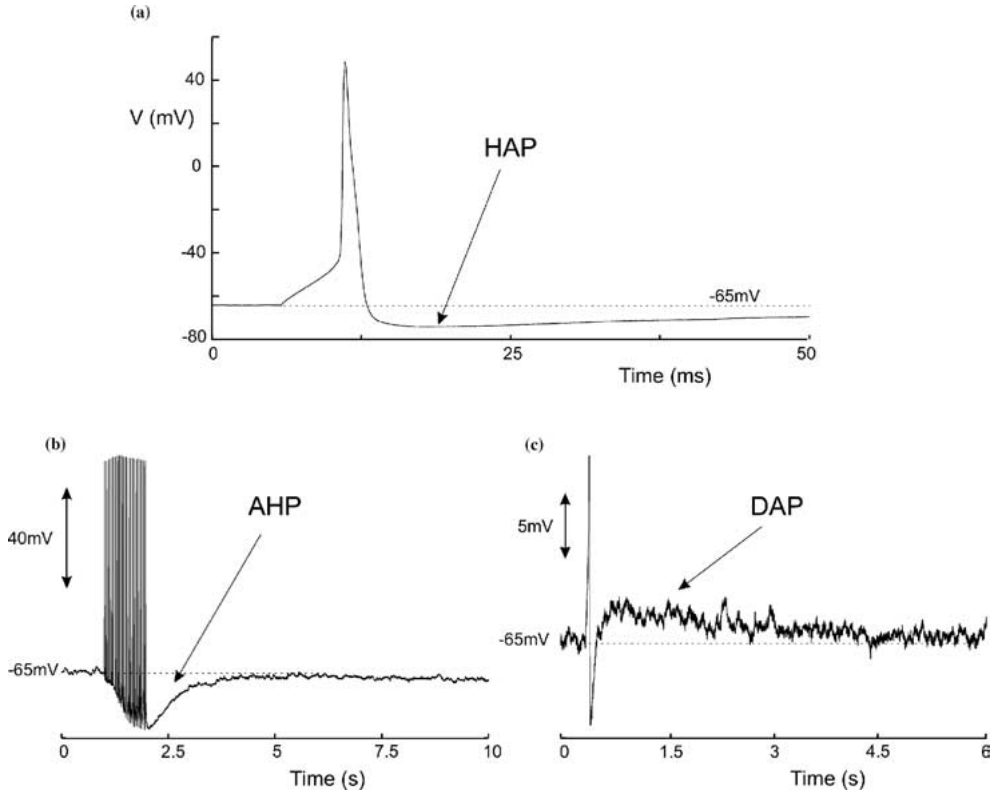

Figure 1. Spike after-potentials in SON MNC's: (a) The hyperpolarized after-potential (HAP) follows each spike and typically hyperpolarizes the cell by $\sim$ 7.5 mV and lasts for 25–125 ms. (b) An after-hyperpolarizing potential (AHP) follows each spike train. It decays mono-exponentially with $\tau \sim 500$ ms and has a maximum amplitude $\sim$12.5 mV. (c) The depolarized after-potential (DAP) is preferentially expressed in AVP cells. DAP's can last for several seconds and a single DAP can depolarize the cell by $\sim$3 mV. Note that the spike has been truncated for clarity. The traces are taken from whole cell (a, b) and sharp electrode (c) recordings in the slice and explant respectively.

cells and less so in OT MNC's (Armstrong et al., 1994). However, it is labile and so its presence or absence does not discriminate cell type.

Trains of spikes also activate a long-lasting hyperpolarization of the membrane potential, the AHP shown in Fig. 1b (Andrew and Dudek, 1984b; Bourque et al., 1985; Armstrong et al., 1994; Kirkpatrick and Bourque, 1996). The AHP decays with a single time constant (400–500 ms) (Armstrong et al., 1994; Teruyama and Armstrong, 2002), is abolished by removal of calcium, and is markedly attenuated by apamin (Bourque and Brown, 1987; Armstrong et al., 1994; Kirkpatrick and Bourque, 1996; Kirkpatrick 1997).

We have constructed a single-compartment mathematical model, based on a set of Hodgkin-Huxley equations, that contains the minimum number of currents and the simplest calcium dynamics needed to reproduce in vitro MNC electrical activity. We explore in particular how the different potassium currents sculpt these after-potentials and show how they contribute to the regulation of excitability in these cells. We also present data from simultaneous calcium fluorescence and electrical recordings to show how electrical activity correlates with calcium elevation and how spike after-potentials relate to intra-cellular calcium transients. We first reconstruct the evoked action potentials and after-potentials shown by a generic SON MNC and we compare the model with cellular activity. We then extend our model to include features specific to first AVP and then to OT cells, and we finally show how these features contribute to aspects of the cells' discharge pattern.

2. Methods

2.1. Electrophysiology

We have borrowed from both sharp electrode and whole cell recordings made in the lab to demonstrate some of

the properties of SON neurones tested in the model. All of the examples used to illustrate these properties have been described in the literature by ourselves and others. Sharp electrode recordings were made from the hypothalamo-neurohypophysial explant preparation (Stern and Armstrong, 1996; Teruyama and Armstrong, 2002). Briefly, virgin adult female rats were deeply anesthetized with sodium pentobarbital (50 mg/kg, i.p.) and perfused through the heart with cold medium in which NaCl was replaced by an equiosmolar amount of sucrose. A ventral hypothalamic explant was removed with iris scissors and placed in an incubation chamber. The incubation medium consisted of (in mM): 25 $NaHCO_3$, 3 KCl, 1.24 NaH_2PO_4, 124 NaCl, 10 glucose, 2 $CaCl_2$, 1.3 $MgCl_2$, and 0.2 ascorbic acid. The medium was saturated with 95% O_2– 5% CO_2, with a pH of 7.3–7.4 and an osmolality of 290–300 mOsm/kg H2O; it was warmed to 33–34°C. Intracellular recording and labeling, signal digitization, and data analysis were made as previously described using sharp electrodes filled with 1.5 M potassium acetate, 0.1 M potassium chloride.

Whole cell recordings were made from 300 μm hypothalamic slices under visual guidance, using procedures similar to those reported by Stern et al. (1999) and Wilson and Callaway (2000). These animals were also perfused under anesthesia (see above) with ice-cold medium before slicing on a vibrating microtome (Campden Inst. VSL, or Leica VT1000S). Pipettes were filled with solution consisting of (in mM): K-gluconate or K-methylsulfate 140, NaCl 4, KCl 8.2, MgCl 0.6, HEPES 10, Mg-ATP 4, Na-GTP 0.3, and EGTA (0.2) (pH 7.4). Recordings were made with either a Neurodata IR283 intracellular recording bridge amplifier or an Axopatch 200B amplifier (Axon Instruments). The effects of 100 nM Iberiotoxin (IbTX) (Sigma/RBI and Latoxon) on spikes were evaluated with a paired t-test. All values in the text are mean ± s.d.

2.2. *Calcium Imaging*

We used calcium imaging to obtain values for the amplitude and decay of calcium transients during spiking. The procedures were similar to those described in Wilson and Callaway (2000). Horizontal slices (300 μm) through the SON of adult, virgin female rat brains were made after anesthesia and perfusion as described above. The extracellular solution consisted of (in mM): 25 $NaHCO_3$, 3 KCl, 1.24 NaH_2PO_4, 124 NaCl, 10 glucose, 2 $CaCl_2$, 1.3 $MgCl_2$, and 0.2 ascorbic acid. Slices were imaged on an Olympus BX50WI microscope using a 40× water immersible lens (0.8 n.a.). The pipette filling solution consisted of (in mM): K-gluconate or K-methylsulfate 135, NaCl 4, KCl 4, HEPES 10, Mg-ATP 1, Na-GTP 1.0, and fura-2 (Na salt) 0.1 (pH 7.4). Recordings were made with a Neurodata IR283 intracellular recording bridge amplifier. High speed fura-2 fluorescence images were obtained using the Imago Sensicam (T.I.L.L. Photonics, Planegg, Germany), with a 12 bit, 640 × 480 chip (readout rate = 12.5 MHz; scale = 0.246 μm/pixel with the 40× objective). For excitation, light of either 340 or 380 nm was provided by a Polychrome II monochromometer (T.I.L.L. Photonics) controlled with analog voltage commands and using a Hammamatsu L2841-01 75W Mercury-Xenon arc lamp. The frame rate was 40–50 Hz, and pixels were typically binned (4 × 4) to increase the signal to noise ratio. Software for data acquisition and analysis is based on that developed and described by Lasser-Ross et al. (1991) and modified by J.C. Callaway, and allowed simultaneous recording of electrical and fluorescence signals from a Computerboards 16 bit A-D board.

Changes in bulk calcium ($[Ca^{2+}]_i$) were estimated by measuring the change in fluorescence intensity at 380 nm (ΔF) divided by a baseline fluorescence (F) to obtain the fractional change in $[Ca^{2+}]_i$, $\Delta F/F$. Baseline fluorescence was first corrected for tissue autofluorescence by subtracting the background fluorescence from a region near the filled cell. The value $\Delta F/F$ was further corrected for bleaching during an exposure by subtracting time matched, filtered (3 Hz) control curves of F at a hyperpolarized holding potential (<-70 mV), where no calcium entry could be detected.

To obtain information about the range of change in absolute $[Ca^{2+}]_i$, we first measured resting $[Ca^{2+}]_i$ in several neurones near −70 mV by the ratioing method (Grynkiewicz et al., 1985) using the following formula:

$$[Ca^{2+}]_i = K_d \frac{R - R_{\min}}{R_{\max} - R} \frac{F380_{\max}}{F380_{\min}} \qquad (1)$$

where R is the 340/380 nm intensity ratio in the neuron corrected for background fluorescence at each wavelength, $R_{\min}$ and $R_{\max}$ are the minimum and maximum ratios from a calibration done on this set-up using Ca^{2+} -EGTA solutions and fura-2 provided by Molecular Probes and diluted in our K gluconate patch solution. The calibration produced a K_d for fura-2 of 226 nM, $R_{\min}$ of 0.416, $R_{\max}$ of 10.37 and $F380_{\max}/F380_{\min}$ of 9.32. The change in Ca^{2+} to a

stimulus was then calculated from $\Delta F/F$ using the following formula, derived by Wilson and Callaway (2000):

$$[Ca^{2+}]_i = -\frac{\frac{\Delta F}{F} K_d + [Ca^{2+}]_{\text{rest}} \left(\left(\frac{\Delta F}{F} - 1\right) \frac{F380_{\max}}{F380_{\min}} + 1\right)}{\frac{1}{K_d}[Ca^{2+}]_{\text{rest}} \frac{\Delta F}{F} \frac{F380_{\max}}{F380_{\min}} + \left(\frac{\Delta F}{F} - 1 + \frac{F380_{\max}}{F380_{\min}}\right)} \quad (2)$$

where $[Ca^{2+}]_{\text{rest}}$ is the resting level measured in that neuron. This formula did not require obtaining a maximal fluorescence change (i.e. by calcium loading). In the text all experimental results will be cited as mean ± s.d.

2.3. Mathematical Model

2.3.1. Electrical Activity. The relative distribution of currents over the cell is unknown and so as a first approximation we model the cell as a single (electrical) point, and neglect spatial effects. While there is evidence that SON dendrites do contribute to electrotonus (Armstrong and Smith, 1990) and are excitable (Bains and Ferguson, 1999), this simplified approach is sufficient to explain the gross aspects of the cell's discharge and allows us to study interactions between currents. We model electrical activity as a Hodgkin-Huxley-type system:

$$\frac{dV}{dt} = -\frac{1}{C}(I_{\text{Na}} + I_{\text{Ca}} + I_K + I_A + I_c + I_{\text{AHP}} + I_{\text{SOR}} + I_{\text{leak}}) \quad (3)$$

where I_{Na} represents the fast sodium current; I_{Ca} a high threshold calcium current; I_K and I_A denote the delayed rectifier and the A-current respectively; I_c and I_{AHP} two calcium-dependent potassium currents; I_{SOR} is the sustained outward-rectifier (Stern and Armstrong, 1995); and I_{leak} is a leak current that accounts for the membrane's passive decay to rest.

All voltage- and calcium-dependent currents have the standard activation/inactivation form:

$$I_\gamma(t) = g_\gamma\, m^\alpha(t)\, h^\beta(t)\, (V - E_{\text{rev}}) \quad \text{or}$$
$$I_\gamma(t) = g_\gamma\, m^\alpha(t)\, (V - E_{\text{rev}}) \quad (4)$$

Where the first equation describes an inactivating, and the second a non-inactivating current, and each current I_γ has conductance g_γ and reversal potential E_{rev}.

Any activation (e.g. $m(t)$) or inactivation ($h(t)$) function $x(t)$ evolves to its equilibrium state x_∞ with time constant τ_x, according to

$$\frac{d}{dt}x(t) = \frac{x_\infty - x(t)}{\tau_x} \quad (5)$$

Wherever possible we have drawn on published values (e.g. Cobbett et al., 1989; Nagatomo et al., 1995) for activation functions and their time constants, however we have had to adjust many of these parameters to build a consistent model. These adjustments have typically been of the order of a <10 mV shift of the midpoint of the activation/inactivation curve, and could be accounted for by differences in experimental protocols (see also Borg-Graham, 1999; Golowasch et al., 2002). The resulting activation and inactivation functions, and their corresponding time constants, are given in the appendix. We have assumed a specific capacitance, $C = \tau/R$, of 1 μF cm^{-2} (Hille, 2001), and fitted conductances (measured in mS cm^{-2}) accordingly.

2.3.2. Electrical Currents

2.3.2.1. Potassium Currents. MNC's express a delayed rectifier, I_K (Cobbett et al., 1989); a transient 'A'-type current I_A (Bourque, 1988; Cobbett et al., 1989; Nagatomo et al., 1995); an AHP current, I_{AHP} (Andrew and Dudek, 1984b; Bourque et al., 1985) which is carried by SK channels (Bourque and Brown, 1987; Kirkpatrick and Bourque, 1995, 1996; Kirkpatrick, 1997); and a voltage- and calcium-dependent potassium current, I_c, (Dopico et al., 1999) which is carried by BK channels. OT-cells, but not VP-cells, also possess a slowly-activating, time- and voltage-dependent, non-inactivating, sustained-outward-rectification (I_{SOR}) (Stern and Armstrong, 1995).

2.3.2.2. Inward Currents. The ubiquitous fast sodium current, I_{Na}, (Cobbett and Mason, 1987) mediates the upstroke of the action potential. I_{Na} has the usual cubic activation and linear inactivation, and parameters have been adjusted to give activity consistent with experiment. We have assumed that I_{Na} activates instantaneously, so that $m(t) = m_\infty$, and that the current reverses at $E_{\text{Na}} = +50$ mV. SON MNC's express several high- and intermediate-voltage activated calcium channels (Fisher and Bourque, 1995; Foehring and Armstrong, 1996; Luther and Tasker, 2000; Joux

et al., 2001), but, in rat, low-threshold currents are inconsistently observed (but see Fisher and Bourque, 1995). As a consequence of their depolarized activations, these calcium currents are only active during an action potential and we therefore approximate the family of Ca^{2+} currents by a single, high-voltage activated, non-inactivating calcium current I_{Ca}.

2.3.2.3. Leak Currents. The leak current models all processes and pumps that comprise the passive response of the membrane. It accounts for the membrane time constant (12–16 ms; Armstrong et al., 1994 and has a reversal potential of $E_{leak} = -65$ mV, and conductance $G_{leak} = 0.083$ mS cm^{-2}

$$I_{leak} = G_{leak}(V - E_{leak}) \tag{6}$$

A significant contribution to I_{leak} is a persistent potassium current, $I_{K,leak}$, that is always active when the cell is at rest (Han et al., 2003). In AVP cells $I_{K,leak}$ appears to have a component that can be modulated by changes in intra-cellular calcium, and this calcium-dependency is also voltage-dependent (Li and Hatton, 1997b). To examine the effects of calcium and voltage on the leak current we will later decompose I_{leak} into a linear combination of a sodium leak current and a potassium leak current.

$$I_{leak} \equiv G_{leak}(V - V_{rest}) = I_{Na,leak} + I_{K,leak} \tag{7}$$

2.3.3. Calcium Concentrations. Our data (see later) suggests that intra-cellular calcium is compartmentalized, possibly by buffering processes. There appear to be (at least) three distinct compartments, each of which activates a single calcium dependent process—I_c, I_{AHP} or $I_{K,leak}$. Rather than investigating a complete spatial model for calcium diffusion in these cells, we model this compartmentalization with three distinct pools of calcium (see also Borg-Graham, 1987). These pools correspond to the local concentrations in three geographically disparate regions, as shown in Fig. 2. Each is homogeneous and for simplicity we assume that there is no diffusion between them. For example, the calcium sensor for a BK channel is located within 1 μm of the calcium channel (Storm, 1993), and senses the rapidly fluctuating calcium concentration in a small domain about the channel (Van Goor et al., 2001). In contrast, the potassium component to the leak current appears to be modulated by the mean somatic (bulk) calcium concentration, $[Ca^{2+}]_i$, (see later)

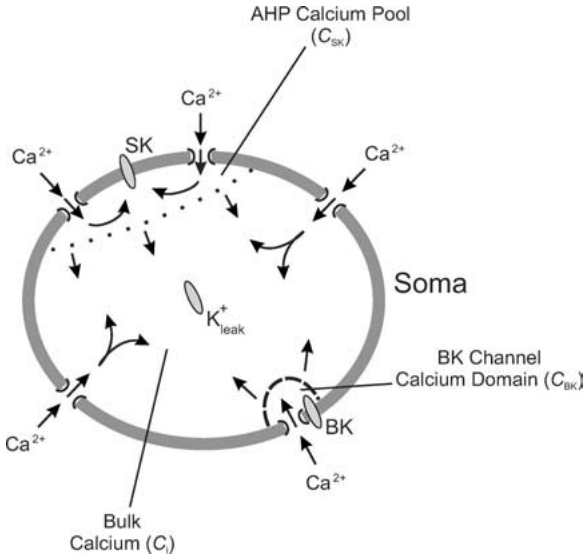

Figure 2. Calcium domains and preferential activation of potassium channels. Ellipses denote the proposed locations of the calcium receptor for the respective channel. We propose that: BK receptors are co-localized with their channel; SK channels are attached to the cell membrane, but distal from the channel; $I_{K,leak}$ receptors are internal to the cell, and so sense bulk and not micro-domain calcium concentrations. (i) Dashed curve indicates putative calcium domain associated with I_c. The BK channel is close to the calcium channel and so experiences a high concentration, rapidly attenuating calcium transient. (ii) Dotted curve denotes domain associated with I_{AHP}. SK channels are further from the Ca^{2+} channel and so are affected by a smaller, slower ($\tau \sim 500$ ms) calcium signal. (iii) The receptors for $I_{K,leak}$ are still further from the site of Ca^{2+} influx and so the current is modulated by bulk calcium rather than some local transient. An example of the relative amplitudes and time-scales of these three transients is shown in Fig. 3.

and does not seem to be affected by localized calcium transients.

Calcium concentrations evolve according to (Plant, 1978)

$$\frac{d}{dt}C_\gamma = -\alpha_\gamma I_{Ca} - \frac{1}{\tau_\gamma}(C_\gamma - C_r) \tag{8}$$

The subscript γ labels the pool of calcium, so that $\gamma = \{BK, SK, i\}$ depending on whether the pool activates I_c, I_{AHP} or $I_{K,leak}$. C_γ denotes the concentration of calcium in that pool; α_γ relates the amplitude of the calcium current to calcium influx, and also reflects the size of each pool; the time constant τ_γ approximates the buffering and diffusion processes that return the calcium transient to rest; and C_r(=113 nM) denotes the basal calcium concentration. The relative evolutions of

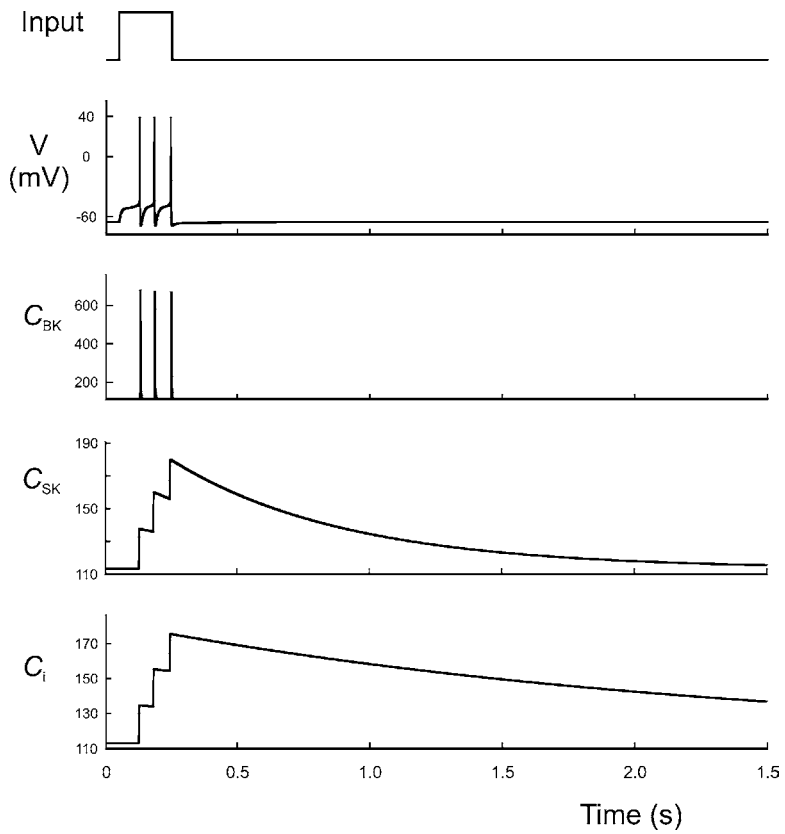

Figure 3. Putative amplitudes and time-scales of model calcium transients (recall Fig. 2) in response to three evoked action potentials. All concentrations are in nM.

each compartment are compared in Fig. 3, and of the three evolution equations will be discussed individually in the text.

This model ignores the fine details of calcium homeostatis, but our intent here is to model and understand the role and dynamics of potassium currents, and the degree to which they are affected by $[Ca^{2+}]_i$. Calcium thus plays a passive role in our analysis, and so we have used a phenomenological model that most simply reproduces its trajectory.

2.4. Numerical Methods

Simulations were undertaken with the differential equation solver XPPaut (Ermentrout, 2002) (downloadable from http://www.math.pitt.edu/~bard/xpp/xpp.html), and several different integration algorithms (e.g. backwards Euler, Dormund-Prince and CVode) and time steps (most frequently $\delta t = 0.017$ ms) were used to check accuracy and stability.

3. Results

3.1. Calcium Concentrations

Calcium is associated with the activation of both BK and SK potassium channels and has also been implicated as a key modulator of the resting potassium leak current, $I_{K,\text{leak}}$ (Li and Hatton, 1997b). Our simultaneous electrical recording and calcium imaging shows that intracellular calcium concentrations in MNC's increase only when the cell is electrically active, and that there is little sub-threshold calcium entry. The largest contribution to calcium increase is probably Ca^{2+} influx through voltage gated channels, but there is also a component due to release from internal stores (Lambert et al., 1994; Li and Hatton, 1997a). However our experimental protocol cannot distinguish between these two sources. Clearance after activity is mediated by extrusion *via* pumps and exchangers, and uptake into mitochondria and intracellular stores (Komori et al., 2001).

The mean basal calcium concentration in the soma is 113 ± 60 nM ($n = 45$), and a single spike transiently raises this by 19.8 ± 6.3 nM ($n = 11$), which then clears mono-exponentially with a time constant of $\tau = 0.99 \pm 0.5$ s, ($n = 11$).

Clearance after trains of spikes is more complex and we used two different protocols to examine the consequent transients. First, to evoke DAP's that were relatively free from contamination by the AHP, we used a 3 spike train at 20 Hz, and varied the membrane potential with continuous current to achieve the largest DAP that was subthreshold to spiking (Armstrong et al., 1994) (left panel Fig. 4a). The calcium transients from individual spikes did not sum linearly, and the calcium increase following 3 spikes at 20 Hz was 43.1 ± 13.2 nM ($n = 15$). In contrast to single spikes, most calcium transients elicited by triplets of spikes at 20 Hz showed a bi-exponential decay with a fast (mean time-constant $\tau_f = 0.33 \pm 0.14$ s, $n = 11/15$) and a slow ($\tau_s = 1.94 \pm 0.95$ s, $n = 15$) component (middle panel Fig. 4a). This suggests that there are two dominant mechanisms contributing to clearance, for example extrusion close to the membrane could provide the faster mechanism, and release and reuptake into intracellular stores (Li and Hatton, 1997a) the slower one. Alternatively these two mechanisms could be the Na^+-Ca^{2+} exchanger and the calcium pump. The presence of a slow time constant for calcium decay depends only on the spiking history and not on presence or absence of the DAP. For example, when a subset of the cells were slightly hyperpolarized to inhibit the DAP, three spikes still evoked calcium transients that decayed with two time constants in 5/7 neurons, and these were not significantly different from those associated with a DAP at more depolarized potentials: 0.28 ± 0.03 s ($n = 5/7$) and 2.28 ± 1.3 s ($n = 7/7$).

We further used trains of 20 spikes at 10 and 20 Hz in order to evoke AHPs (Kirkpatrick and Bourque, 1996) and examined the associated calcium transients (Fig. 4b). Although some neurons revealed two time constants in this protocol, the faster τ was small and inconsistent even within a neuron, so we estimated the decay from a single exponential. In contrast to single spikes or short (3 spike) trains, the time constants after these longer trains had a leftwardly skewed distribution, and the mean (2.78 ± 1.1 s) was discrepant from the median. Given this skew, it is worthwhile considering the median value, which was 2.33 s.

The median AHP time constant, 656 ms, that we determined in this protocol is close to those that we have reported previously (400–500 ms) in normal rats with sharp electrode recordings (Armstrong et al., 1994; Stern and Armstrong, 1996; Teruyama and Armstrong, 2002), and from Fig. 4 it is clear that while the clearance of bulk calcium is tracked by the time-course of the DAP, it is dissociated from the decay of the AHP. A similar dissociation has been noted in CA1 pyramidal cells (Jahromi et al., 1999), (but cf. Lancaster and Zucker, 1994; Lasser-Ross et al., 1997). We propose that in MNCs this anomaly is caused by cytosolic Ca^{2+} compartmentalization (Chad and Eckert, 1984; Simon and Llinas, 1985; Van Goor et al., 2001), and that the calcium sensor for each AHP channel is distant from site of influx but close to the cell membrane (see e.g. Yuen and Durand, 1991; Sah 1992). It therefore experiences a global calcium concentration, but can be rapidly affected by membrane pumps and diffusion and so the domain around it decays more quickly than does the bulk calcium. Alternatively it is possible the AHP/$[Ca^{2+}]_i$ dissociation represents a morphological segregation such that the AHP channels are confined to the dendrites and experience a faster transient due to higher surface to volume ratios (cf. Wilson and Callaway, 2000). However, while we have found that dendritic calcium transients do generally decay faster (data not shown), they rarely match the decay of the AHP. In addition our preparation (300 μm slice) typically includes a limited dendritic contribution, and furthermore even fully deafferented cells still possess a substantial AHP (see e.g. Fig. 8 of Oliet and Bourque, 1992).

We treat the bulk calcium and the calcium domain surrounding each AHP channel as being two distinct, and disconnected, compartments (see Fig. 2) whose calcium concentrations are denoted C_i and C_{SK} respectively, and which both evolve according to Eq. (8). We have adjusted the pre-factor α_i to fit the rise amplitude (19.8 nM per spike), and the pre-factor α_{SK} to fit the activation of the AHP. We have set the decay time-constant for the AHP compartment to be equal to the median AHP decay time-constant, i.e. $\tau_{SK} = 656$ ms, and to further simplify the model we have used a single, slow, time-constant for bulk calcium decay, $\tau_i = 2.33$ s. The evolution of each compartment in response to a short spike train is shown in Fig. 3, and is compared with that of C_{BK}, the micro-domain surrounding each BK channel. Note that as the volume

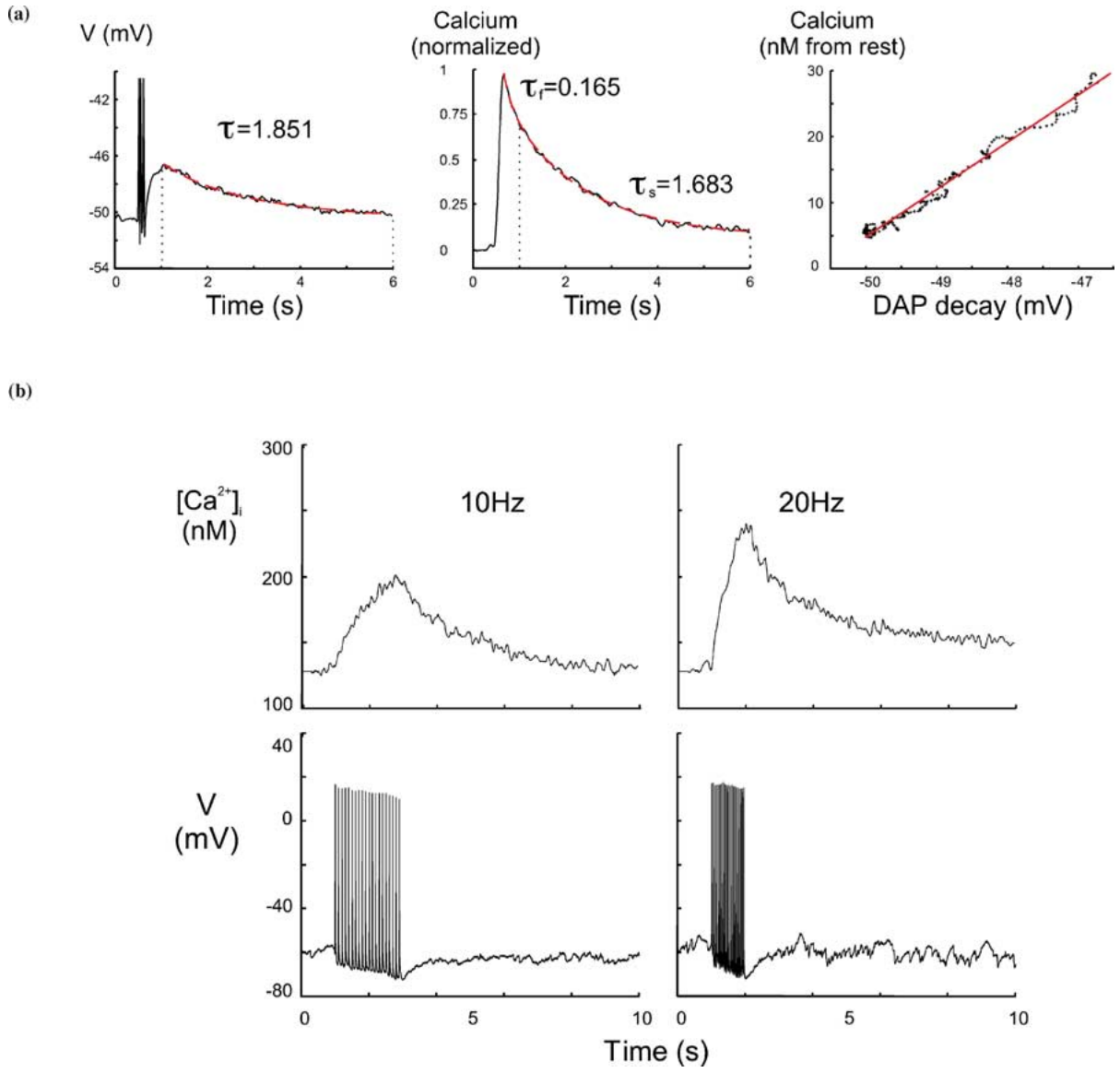

Figure 4. (a) Left Panel: An average of 15 DAP's from different neurons evoked with 3 spikes at 20 Hz. The baseline membrane potential was offset to be near −50 mV for all cells to reduce DAP amplitude variability and obtain a smooth decay. The decay was fit to a single exponential of 1.851 s. Middle Panel: The average somatic calcium response for the 15 DAP's. Each response was normalized to its peak. This curve was fit with a double exponential with a fast time constant of 0.165 s and a slow time constant of 1.683 s. The vertical lines show the region of this curve (i.e. $1 \leq t \leq 6$ s) matching the DAP decay shown in the left panel. Right Panel: The decay of the averaged DAP is plotted against the average Ca^{2+} decay. For calcium, values were converted to nM using the average peak value (41 nM) in order to appreciate the relationship between elevations in bulk calcium and the activation of the DAP. The linear fit to these responses is shown. (b) Calcium rise and clearance for trains of evoked spikes at 10 Hz and 20 Hz. Clearance is mono-exponential and independent of frequency ($\tau \sim 2.4$ s). Data taken from whole cell recordings from the SON of a hypothalamic slice.

of the domain decreases (recall Fig. 2), the maximum amplitude of the transient increases but decays more quickly, as one should expect from surface-to-volume considerations.

3.2. I_A and I_K: Spike Repolarization and Overshoot

The transient outward current, I_A, (Bourque, 1988; Cobbett et al., 1989; Nagatomo et al., 1995) has a

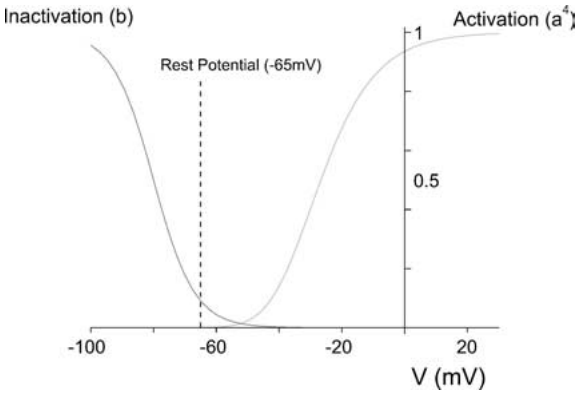

Figure 5. Activation and inactivation of the *A*-current. The current is significantly inactivated at rest, and completely inactivated by a depolarization of ∼10 mV. Inactivation can be removed by a conditioning hyperpolarization.

quartic activation and a linear inactivation (i.e. $\alpha = 4$, $\beta = 1$ for Eq. (4)), while the delayed rectifier, I_K, is a non-inactivating current with a cubic activation (Cobbett et al., 1989). I_A is significantly inactivated at rest (−65 mV) and almost completely inactivated by a depolarization to −60 mV (see Fig. 5). In MNCs, I_A is blocked by 4-aminopyridine (4-AP), but not by tetraethylamonium (TEA), while the opposite is true for I_K, and so these currents can be distinguished by their pharmacology.

Spikes evoked from rest are significantly broadened by the application of either 1 mM 4-AP (Bourque, 1988) or TEA (Bourque and Renaud, 1988) but their widths are unaffected by 10 nM charybdotoxin (Dopico et al., 1999), implying that both I_A and I_K but not I_c mediate spike repolarization. These protocols can be simulated in the model by setting either G_A or G_K to be zero, and the resulting effect on spike width is shown in Fig. 6. The relative contribution of each current to repolarization depends upon the degree of inactivation of I_A, and hence the holding potential, and so spikes evoked from a depolarized holding potential will be broader than those evoked from a more hyperpolarized one. The HAP depends on I_A (Bourque, 1988; Bourque et al., 1998), and in the model this is caused by I_A overshooting the rest potential. However the HAP also has a component that depends on I_c and this will be examined later.

3.2.1. I_A and Spike Latency. A conditioning hyperpolarization to <-75 mV removes inactivation of I_A (Fig. 5) and delays the occurrence of the first spike when the cell is subsequently depolarized (Bourque, 1988; Fisher et al., 1998; Fisher and Bourque, 1998) (see Fig. 7), and this latency is abolished by 6 mM 4-AP (Bourque, 1988; Stern and Armstrong, 1997). The rapid activation of I_A appears as a knee on the fast rising phase of the depolarization, and develops

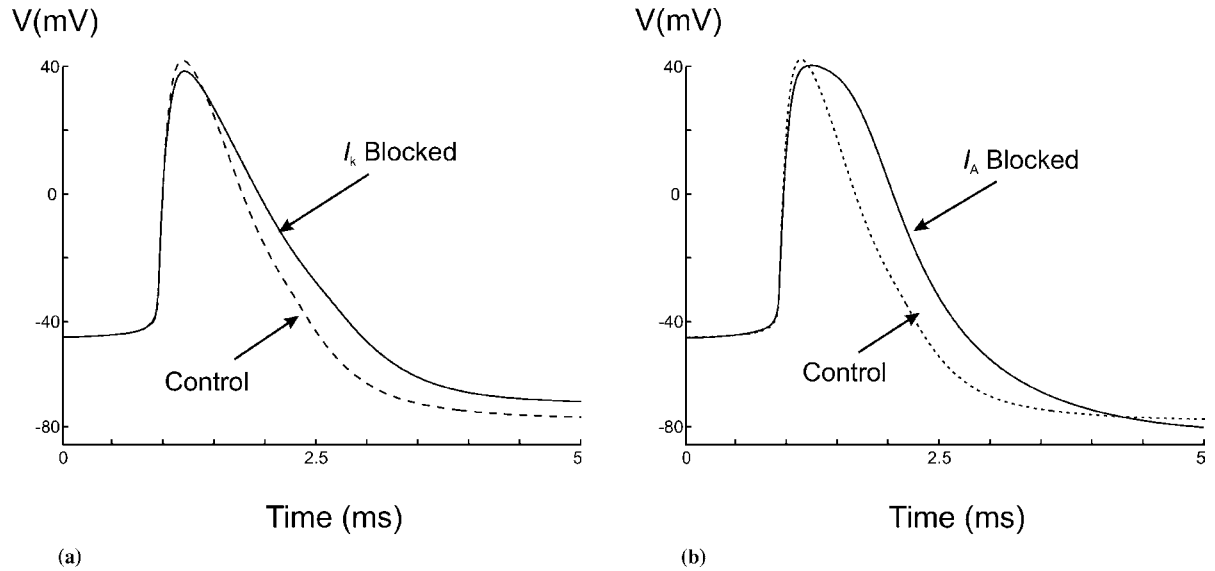

Figure 6. Both I_K and I_A contribute to spike repolarization, and pharmacological block of either current significantly broadens the action potential (Bourque, 1988; Bourque and Renaud, 1988). The effects of TEA and 4-AP are reproduced in the model by (a) setting $G_K = 0$ and (b) setting $G_A = 0$ (cf. Fig. 12 of Bourque, 1988).

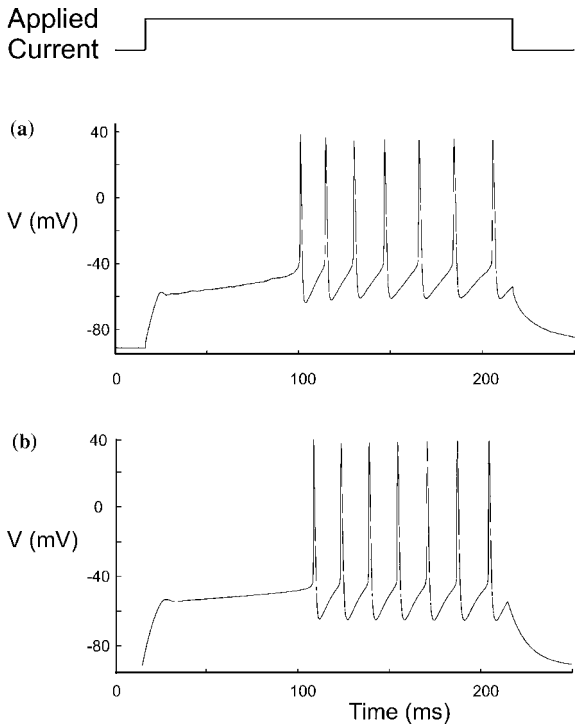

Figure 7. Inactivation of A-current and latency to spiking—(a) experiment, (b) model. Cell given a conditional hyperpolarization to remove inactivation of I_A. Note initial rapid rise of membrane potential, followed by notch due to activation of I_A and subsequent slow depolarization as I_A inactivates. Experimental trace from a whole cell recording from the SON in a hypothalamic slice.

into a notch as the magnitude of the hyperpolarization increases. The slower rise of the potential after the initial rapid activation reflects *A*-current inactivation and the consequent removal of the hyperpolarizing current. This protocol is successfully reproduced by the model (Fig. 7).

3.3. I_{AHP}: Spike Frequency Adaptation and the AHP

The AHP following trains of spikes has a maximum amplitude ∼12.5 mV, decays with a time constant of 400–500 ms, and is activated only by calcium and not voltage (Bourque and Brown, 1987; Armstrong et al., 1994; Kirkpatrick, 1996; Kirkpatrick, 1997) (see Fig. 1b). Associated with AHP activation during a spike train is a progressive increase in the inter-spike interval, which is termed spike frequency adaptation (SFA). Both SFA and the AHP are abolished by removal of calcium, and markedly attenuated by apamin (Bourque and Brown, 1987; Armstrong et al., 1994; Kirkpatrick and Bourque, 1996; Kirkpatrick, 1997), and so both are caused by the activation of calcium-dependent SK potassium channels (Vergara et al., 1998). A third calcium-dependent after-hyperpolarization, slower and weaker than the AHP, has been described (Greffrath et al., 1998) but will not be included here.

Our simultaneous voltage and calcium measurements suggest that the AHP is progressively activated by increasing calcium, (see Fig. 4b), however the calcium dependence of I_{AHP} has not been quantified for MNC's. In other preparations it is described as a non-inactivating current, with a quadratic activation, $q(C_{\mathrm{SK}})$, that follows a Boltzman function (Yuen and Durand, 1991; Aradi and Holmes, 1999), such that

$$q_\infty(C_{\mathrm{SK}}) = \left(1 + \exp\left[-1.120 - 2.508 \log\left(\frac{C_{\mathrm{SK}} - C_r}{1000}\right)\right]\right)^{-1} \quad (9)$$

where C_{SK} denotes the concentration in the AHP calcium domain, and C_r(=113 nM) the resting calcium concentration. We assume that the current activates instantaneously (i.e. $q \equiv q_\infty$) since calcium dynamics are already slow, and so

$$I_{\mathrm{AHP}} = G_{\mathrm{AHP}}\, q_\infty^2 (V - E_K) \quad (10)$$

Once activity has ceased, the AHP decays sharply, typically within 30 ms of cessation of the spike train (Greffrath et al., 1998). Thus q does not saturate, or reach a plateau, during normal activity. If calcium were to saturate q, the AHP would not decay immediately, but would instead initially show a lengthy, flat hyperpolarization which would persist until calcium decayed beyond the point of saturation.

The decay of the AHP can be fit to a single exponential for the majority of AVP cells and roughly half of all OT cells (Teruyama and Armstrong, 2002). An expression for decay may be derived by applying the chain rule to Eq. (9), so that $\dot{q} = \dot{C}_{\mathrm{SK}}\, \mathrm{d}q/\mathrm{d}C_{\mathrm{SK}}$. If calcium decay is also mono-exponential (recall that τ_s dominates clearance) then $\mathrm{d}q/\mathrm{d}C_{\mathrm{SK}}$ must remain constant, and so $q(C_{\mathrm{SK}})$ must be approximately linear for most of the decay. Thus the activation of I_{AHP} must be confined to the (approximately) linear portion of the activation curve, and so $0 < q^2 < 0.35$ (see Fig. 8), implying that C_{SK} must be bounded, possibly by buffering and reuptake mechanisms. A significant fraction of OT cells show a bi-exponential AHP decay, and this variation

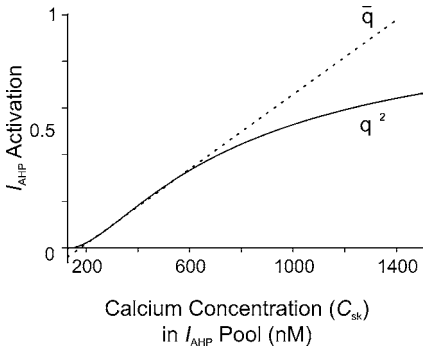

Figure 8. Activation of I_{AHP} as a function of calcium concentration, C_{SK}. Bold curve shows steady-state activation q^2_∞ (see Eq. (9)), and dashed line ($\bar{q}$) is a linear fit to q^2_∞. The model indicates first that the AHP does not saturate, and second that for mono-exponential decay of the AHP, q^2 must be confined to the linear region, thus $q^2_{max} < 0.35$.

could be explained if q has a higher upper bound for OT cells and so departs further from linearity.

C_{SK} evolves according to Eq. (8), and has decay constant $\tau_{\mathrm{SK}} = 656$ ms. We have chosen the step-size, $\alpha_{\mathrm{SK}} = 1.6$, to match the observed progression of spike-frequency adaptation during a spike-train.

The conductance G_{AHP} is now determined by the amplitude of current needed to hyperpolarize the cell by the maximum AHP amplitude when $q^2 = 0.35$. For MNC's in normal animals, the mean maximum AHP across cell types is ~12.5 mV, (Armstrong et al., 1994; Stern and Armstrong, 1996), and so $G_{\mathrm{AHP}} = 0.18$ mS cm^{-2}.

Comparisons between experimental data and the model are shown in Fig. 9 both for the AHP and for spike frequency adaptation.

3.4. I_c and the HAP

The fast, calcium- and voltage-dependent K^+ current, I_c, is carried by BK channels, whose steady-state activation, $p_\infty(C_{\mathrm{BK}}, V)$, can be factored into the product of a Hill- and a Boltzman-function (Dopico et al., 1999):

$$p_\infty = \left[1 + \frac{470}{C_{\mathrm{BK}}^{2.38}}\right]^{-1} \left[1 + \exp \times \left(\frac{\left(-V - 140 \log_{10} C_{\mathrm{BK}} + 370\right)}{7.4}\right)\right]^{-1} \quad (11)$$

where C_{BK} denotes the calcium concentration in the pool sensed by the BK channel. Dopico et al. (1999) determined mean open- and close-times for a single somatic BK channel, and so an activation time constant for I_c may be derived from their data (Hille, 2001), such that $\tau_p = 1.22$ ms .

Block of BK channels with 100 nM iberiotoxin (IbTX) shows that I_c is significantly activated during a single calcium spike (see Fig. 8b of Stern and Armstrong, 1997). However, while Eq. (11) suggests that I_c can only be activated by very elevated calcium concentrations (half-activation = 470 nM), our data (recall Fig. 4) indicates that such bulk concentrations are only achieved after prolonged bouts of activity. We therefore propose that, since the calcium sensor for each BK channel is typically less than 1 μm from a calcium channel (Storm, 1993), each BK channel is activated by calcium in small region close to the channel and not by bulk calcium (see also Chad and Eckert, 1984; Dopico et al., 1999; Van Goor et al., 2001). Such small domains can experience large, rapidly attenuating, calcium transients, and we model the dynamics of C_{BK} with Eq. (8), with $\gamma = BK$. Since I_c is only activated during strong depolarization, e.g. during a spike, the exact time course of C_{BK} does not affect the spiking dynamics and so we assume that C_{BK} decays fully between spikes with a time constant of 1 ms.

Repolarization of the action potential in other vertebrate preparations typically has a component carried by I_c (Adams et al., 1982a; Storm, 1987; Shao et al., 1999; Warman et al., 1994). Our previous data (Stern and Armstrong, 1997) only concerned calcium spikes and furthermore Dopico et al. (1999) investigated dissociated cells, and so we re-examined the effect of I_c blockade on spike repolarization with 100 nM IbTX in ten neurons using whole cell recording (Fig. 10). We find that blocking I_c slightly but significantly increases width at the base of spike by a mean difference of 0.11 ms ($p < 0.02$), but has little effect at half-amplitude ($p < 0.13$). No effects were observed on spike height or rise time. Therefore repolarization is mediated by other currents (e.g. I_A and I_K), and I_c only becomes active toward the end of the spike, which is compatible with the results of Dopico et al. (1999).

In contrast, block of I_c significantly decreases the HAP amplitude by ~2 mV ($p < 0.03$) and hastens its decay by ~13 ms ($p < 0.006$) (Fig. 10). We therefore infer that the HAP has two components: the first is caused by I_A and I_K overshooting rest and hyperpolarizing the cell, but the after-potential is then enhanced and sustained by the late activation of I_c. The effects

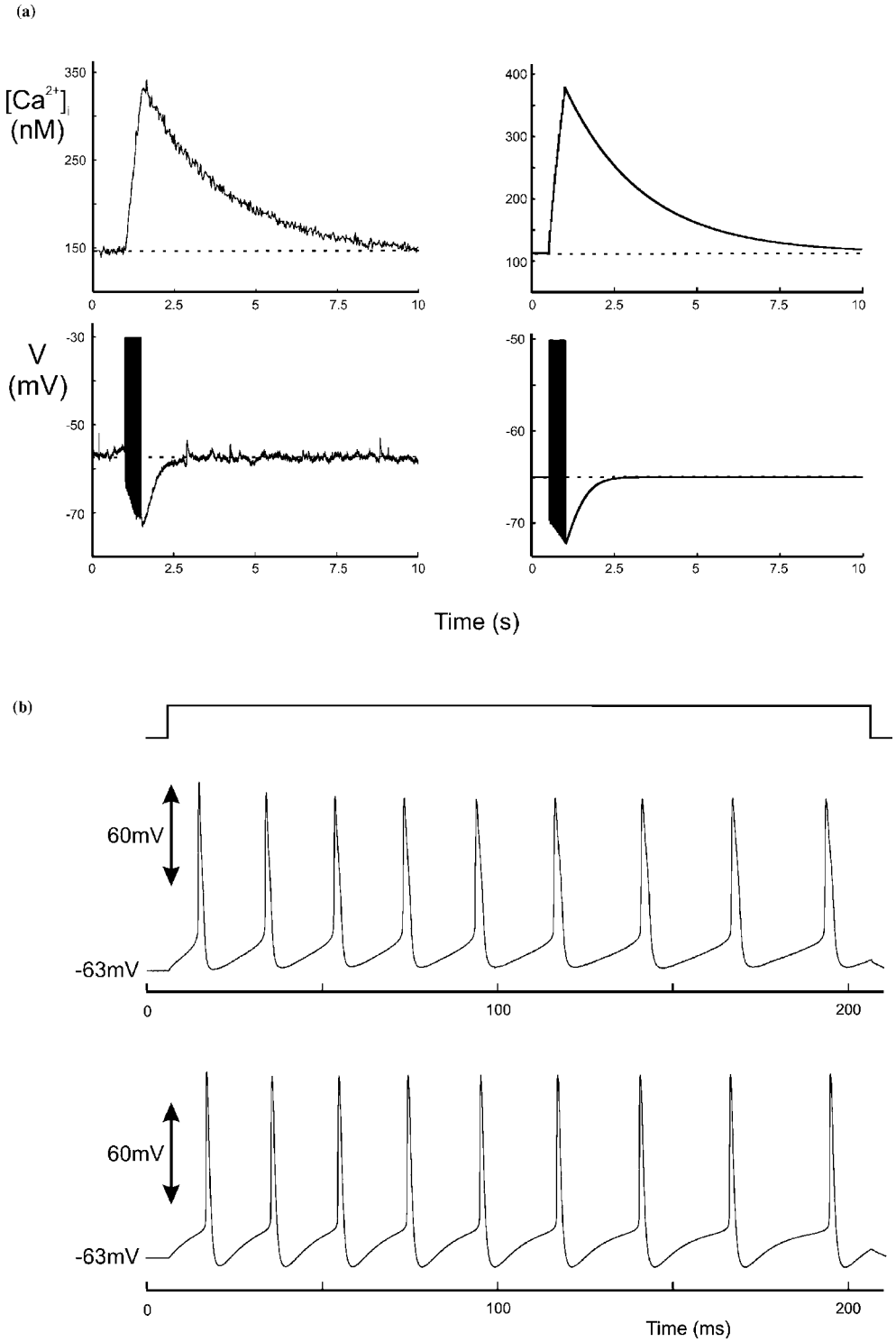

Figure 9. (a) Activation of AHP versus bulk calcium increase, both experiment (left) and model (right) stimulated at 40 Hz with 5 ms pulses. Note that spikes have been clipped for clarity. (b) Spike frequency adaptation: experiment shown above, model below. Note that both cell and model are held depolarized by ∼3 mV to fully inactivate I_A. Experimental data taken from whole cell recordings from the SON in a hypothalamic slice.

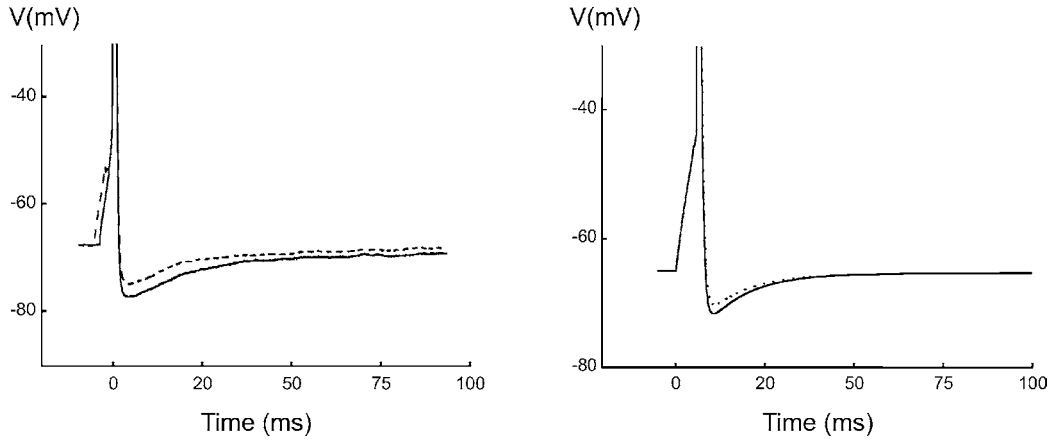

Figure 10. The effect of pharmacological block of I_c with 100 nM IbTX, and simulation of block by setting $G_c = 0$ in the model. Left panel shows experiment, right panel shows model. Spike evoked with 3 ms depolarizing pulse and hence the initial ramp prior to spiking. Bold line shows control, dashed line shows block of I_c. The HAP is still extant when I_c is blocked because I_A and I_K still overshoot the rest potential, but it decays faster and is reduced in amplitude. Experimental data taken from a whole cell recording from the SON in a hypothalamic slice.

of application of IbTX in vitro are compared with the model in Fig. 10.

3.5. $I_{K,leak}$ and the Depolarizing After-Potential

The DAP typically lasts for a few seconds, and transiently lifts the potential to ∼3 mV above rest, although its maximum amplitude depends strongly upon voltage (Bourque, 1986; Li and Hatton, 1997b). DAP's therefore briefly elevate the probability that incident excitation following the initial HAP will trigger a second spike. If the cell does fire again then the DAP following the second spike sums with the residue of the first to produce a much larger depolarization (Andrew and Dudek, 1984a). Importantly, for AVP neurones DAP summation appears to underlie a plateau potential that drives bursts of activity (Andrew and Dudek, 1983; Roper et al., 2001, 2003). The DAP depends strongly on both voltage (Bourque, 1986; Li and Hatton, 1997b) and calcium (Andrew and Dudek, 1984a; Bourque, 1986; Li et al., 1995). The DAP amplitude is maximum when the holding potential is ∼10 mV below threshold, and its amplitude decreases to zero as the holding potential is hyperpolarized below this level (see for example Fig. 3 of Li and Hatton (1997b). This voltage dependence does not solely derive from the ohmic driving force since DAP's vanish at ~ -70 mV rather than at the K^+ reversal potential ($E_K = -96$ mV; Bourque (1988)). In addition: (i) chelation of $[Ca^{2+}]_i$; (ii) blockade of Ca^{2+} channels; (iii) blockade of calcium release from stores; and (iv) removal of extra-cellular Ca^{2+} all inhibit the DAP (Li et al., 1995). In contrast: (i) a single calcium spike can trigger a DAP when I_{Na} is blocked with TTX (Andrew and Dudek, 1984a); (iii) enhancement of calcium release from stores with caffeine amplifies the DAP (Li and Hatton, 1997a); and (iii) application of antibodies to the calcium buffer calbindin can unveil a DAP in a neurone that would not otherwise express one (Li et al., 1995). Finally, our simultaneous electrical recording and calcium fluorescence shows that DAP evolution closely follows that of intra-cellular calcium (recall Section 3.1 and Fig. 4).

A mechanism underlying the DAP is thought (Li and Hatton, 1997b) to be a Ca^{2+}-mediated modulation of a resting K^+ current, possibly TASK-1 (North, 2000; Brown, 2000), which produces a brief depolarizing shift of the cell's resting potential. A related, but distinct, mechanism has been proposed to underlie the depolarized after-potential in neocortical neurones (Greene et al., 1994), and the inhibition of a potassium leak underlies both the cooling-induced depolarization in thermally responsive dorsal root ganglion cells (Reid and Flonta, 2001) and the light-induced, persistent depolarization observed in *Hermissenda* type B photoreceptors (Blackwell, 2002). However note that Bourque et al. (Bourque, 1986; Ghamari-Langroudi and Bourque, 2002) have proposed that the DAP is instead driven by the activation of a non-specific cation (NSC) current rather the modulation of a resting potassium current. We consider this alternative mechanism, and its implications, in (Roper et al., 2003) and we have

shown that the two models are formally equivalent provided that the NSC current is partially activated at rest and is modulated by calcium in a similar manner to that described above.

To model the DAP we first follow McCormick and Huguenard (1992) and subdivide I_{leak} into two linear components: a sodium leak $I_{\text{Na,leak}}$ (Lancaster, 1991) and a potassium leak $I_{K,\text{leak}}$, according to Eq. (7). However we further allow $I_{K,\text{leak}}$ to be modulated by both C_i and V. Since the DAP represents a calcium- and voltage-dependent reduction in $I_{K,\text{leak}}$, we may write this current as

$$I_{K,\text{leak}} = G_{K,\text{leak}}(1 - f([\text{Ca}^{2+}]_i\,, V))[V - E_K] \quad (12)$$

and so

$$I_{\text{leak}} = G_{\text{Na,leak}}[V - E_{\text{Na}}] + G_{K,\text{leak}}(1 - f)[V - E_K] \quad (13)$$

(where $E_{\text{Na}} = 49.5$ mV (Cobbett and Mason, 1987) and $E_K = -96$ mV (Bourque, 1988)). The maximal conductances $G_{\text{Na,leak}}$ and $G_{K,\text{leak}}$ may be determined from: the resting membrane potential $V_{\text{rest}} = -65$ mV, the membrane time-constant $\tau = \mathcal{C}/G_{\text{leak}} = 12$ ms (these measurements are an average of those measured by Stern and Armstrong (1996)), and the boundary condition $\dot{V} = 0$ at $V = -65$ mV. From which it follows that $G_{\text{Na,leak}} = 0.018$ mS cm^{-2} and $G_{K,\text{leak}} = 0.066$ mS cm^{-2}.

Although $(1 - f(C_i, V))$ describes the modulation of a K^+ -leak conductance, it is simpler to think of f as being an *activation* function for the DAP. Neither the form nor the time-course of f is known, but as a first approximation we assume that its steady state value can be written as

$$f_\infty(C_i, V) = \lambda + \Gamma a_\infty(C_i) b_\infty(V) \quad (14)$$

where λ and Γ are constants, with $\lambda + \Gamma = 1$, that account for the possibility that $I_{K,\text{leak}}$ is only partially inhibited. For simplicity we will assume that $\Gamma = 1$, $\lambda = 0$ here. The calcium- and voltage-dependent activation functions are given by

$$a_\infty(C_i) = \tanh\left(\frac{C_i - C_r}{k_a}\right) \quad \text{and}$$
$$b_\infty(V) = \left[1 + \exp\left(-\frac{V + V_b}{k_b}\right)\right]^{-1} \quad (15)$$

where $k_a = 50$ nM, $k_b = 8$ mV, $V_b = -60$ mV and the resting calcium concentration is $C_\tau \equiv [\text{Ca}^{2+}]_{\text{rest}} =$ 113 nM. We have chosen this functional form and parameters to fit the experimental data for the voltage- and calcium-dependence of the DAP. However, up to a translation and scaling factor, our predicted calcium dependence ($a_\infty(C_i)$) is very close to that measured by Selyanko and Sim (1998) for resting potassium currents in cultured rat hippocampal pyramidal neurones. To account for the slow time-to-peak ($\sim$0.3 s) we assume the calcium response to be slow but the voltage response to be instantaneous, and so a obeys Eq. (5) with $\tau_a = 75$ ms. The DAP activation function, f_∞, is graphed in Fig. 11 and comparisons between model DAP's and experiment are shown in Fig. 12.

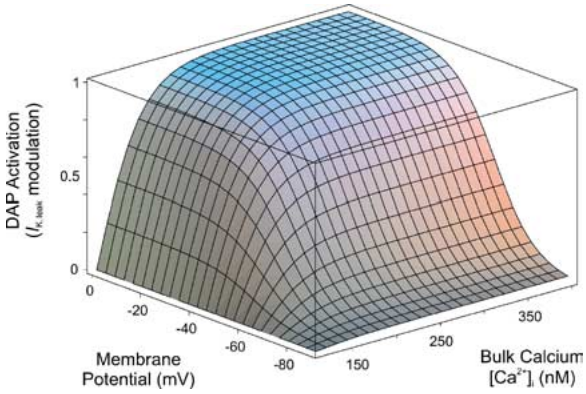

Figure 11. Putative steady-state voltage- and calcium-dependent modulation of the potassium leak current, $I_{K,\text{leak}}$ (see Eq. (14)).

3.6. I_{SOR} and Rebound Firing

Oxytocin cells exhibit a sustained outward rectification (SOR) that becomes active when the cell is held close to threshold (Stern and Armstrong, 1995, 1996, 1997). Underlying the SOR is a potassium current (I_{SOR}) that is similar to the more common M-current (Adams et al., 1982b), but is insensitive to muscarine, and is also distinct (Stern and Armstrong, 1997) from the hyperpolarization-activated non-specific cation current, I_h (Ghamari-Langroudi and Bourque, 2000). This current is not strongly expressed by AVP neurones, and so a test for its presence reliably discriminates cell types in vitro. The effect of I_{SOR} is seen most clearly when the current is first activated and then allowed to de-activate. This is done by current-clamping the cell close to threshold, and then applying a lengthy hyperpolarizing pulse to below the current threshold (Stern and Armstrong, 1995). I_{SOR}

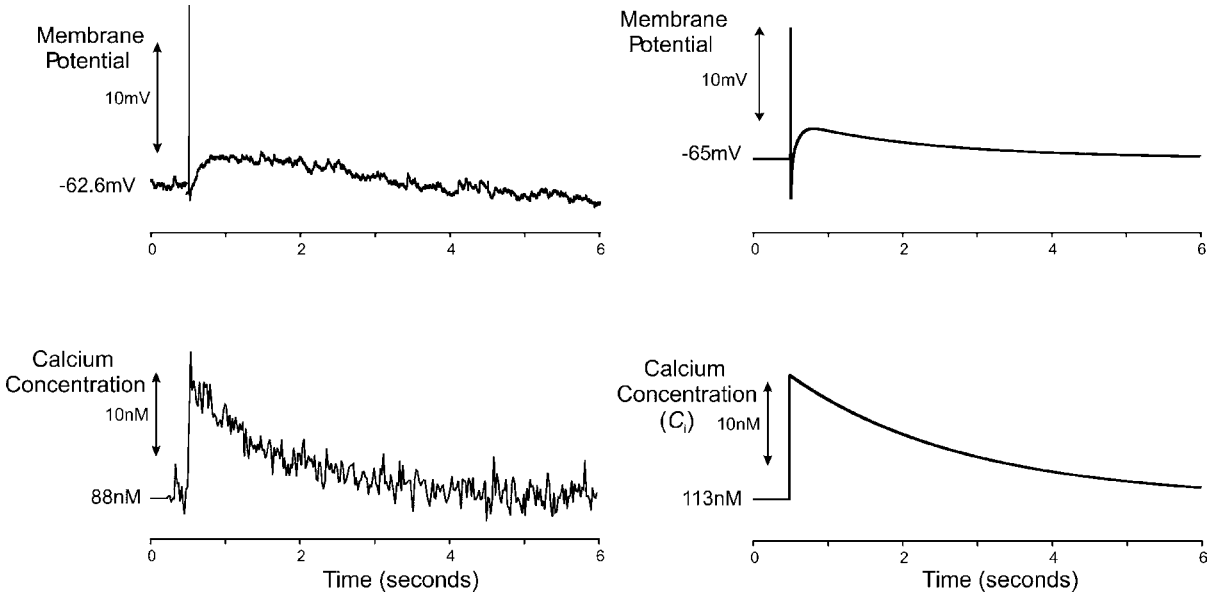

Figure 12. Experimental (left) and model (right) DAP's and their associated calcium transient. Spikes are evoked by a 5 ms depolarizing pulse and have been truncated for clarity. Experimental data taken from whole cell recordings from the SON of a hypothalamic slice.

de-activates slowly and the membrane depolarizes as it does so, and so the signature of this current is an exponentially depolarizing sag to the voltage trajectory, as shown in Fig. 13a. (Note that the amplitude of the depolarizing sag becomes diminished as the hyperpolarization approaches the potassium reversal potential). Subsequent removal of the hyperpolarizing stimulus allows the membrane potential to recover. However because re-activation of I_{SOR} is also slow, the voltage then transiently over-shoots the holding potential and gives rise to a brief, post-inhibitory, rebound depolarization (RD). The RD quickly decays as I_{SOR} reactivates, but can be of sufficient magnitude to sustain a brief volley of action potentials.

When recorded in the presence of TTX, the RD appears as a transient depolarization of the membrane. Its maximum amplitude follows a bell-shaped function of the amplitude of the preceding hyperpolarizing pulse (Stern and Armstrong, 1995), first increasing with hyperpolarization until it reaches a maximum of $\sim$10 mV at a holding potential of ~ -65 mV, and thereafter decreasing. Application of 6 mM 4-AP significantly enhances the RD and eliminates its decrease at hyperpolarized potentials (Stern and Armstrong, 1997), indicating that reduction of the RD is due to removal of inactivation of I_A. The model shows a similar dependency of the RD amplitude, and Fig. 13b demonstrates that the number of rebound-evoked spikes first increases and then decreases for increasing hyperpolarizations. Following the decrease, the number of evoked spikes in some cells will then saturate with increasing hyperpolarization, while in others it decreases to zero (data not shown). The amplitude of the RD in a particular cell, and the corresponding number of spikes, likely depends on the relative contributions of I_A and I_{SOR}.

This current has not yet been characterized in voltage clamp, and so the voltage dependence and time constants of its activation have not been determined. However measurement of the RD amplitude from increasing hyperpolarizations in the presence of 6 mM 4-AP (to block I_A) shows that the current begins to activate close to -65 mV and becomes fully active at ~ -50 mV (see Fig. 7D of Stern and Armstrong (1997)). We have therefore assumed first-order kinetics with sigmoidal activation, and half-activation -60 mV. Activation and de-activation of I_{SOR} appear to have different time constants since the depolarizing sag can be fit to a single exponential, $\tau = 0.39$ s, while the RD decays with time constant, $\tau_1 = 0.26$ s and $\tau_2 = 0.21$ s (Stern and Armstrong, 1995). However distinct time constants for activation and de-activation are not easily incorporated into the Hodgkin-Huxley formalism and so for simplicity we have taken the activation time constant to be $\tau_{\mathrm{SOR}} = 0.26$ s, and note that this is significantly slower than the activation of any other current.

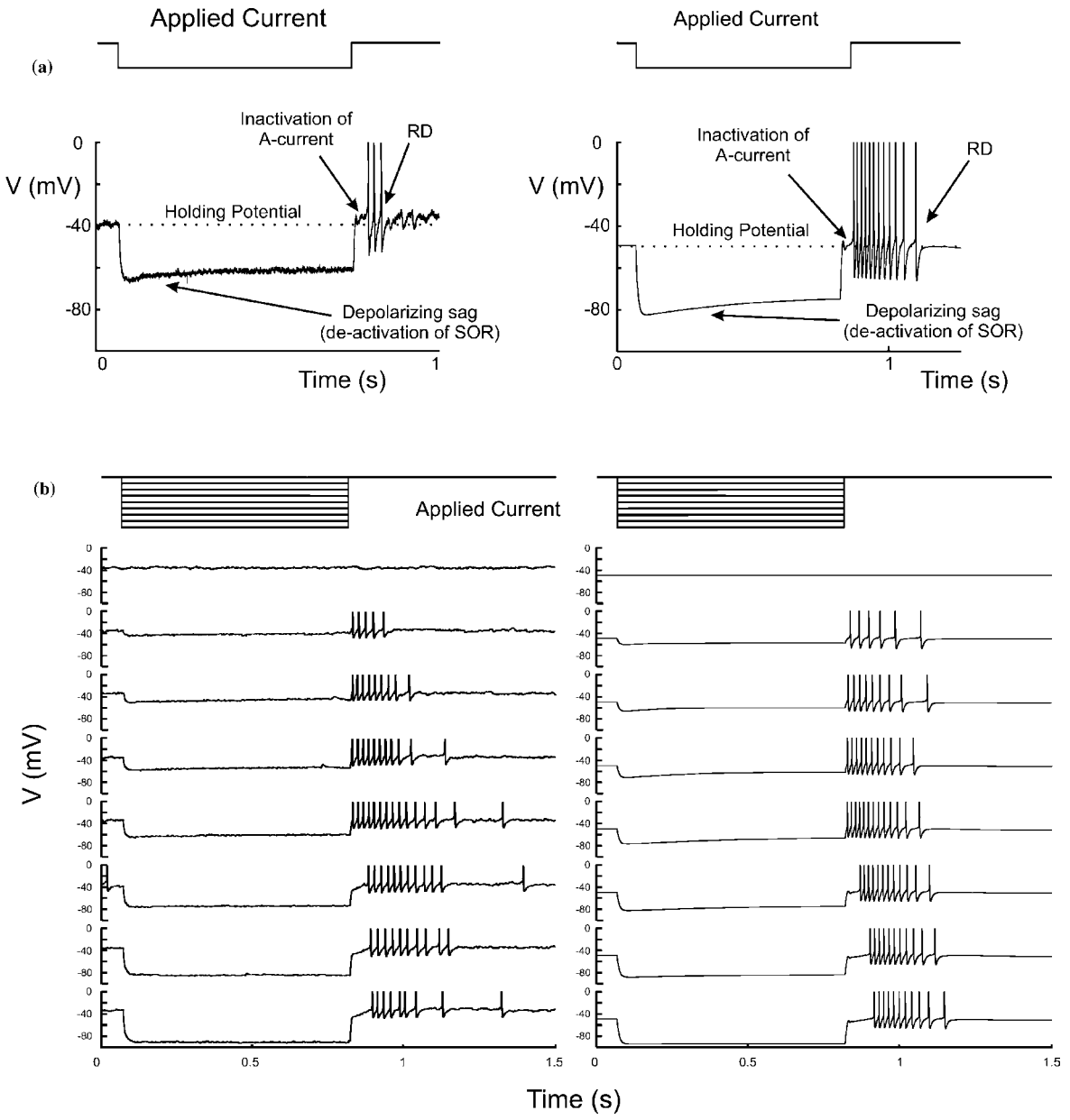

Figure 13. Sustained outward rectification (SOR) and rebound depolarization (RD), right panel model, left panel experiment. (a) I_{SOR} is activated when V is held close to spike threshold and slowly de-activates when a hyperpolarizing pulse is applied—note consequent depolarizing sag to voltage trajectory. I_{SOR} remains transiently de-activated when the hyperpolarizing pulse is released and the cell expresses a brief rebound depolarization (RD) which can support a short spike train. (b) The magnitude of the RD follows a bell shaped function of the hyperpolarization, first increasing as de-activation becomes complete and then decreasing as I_A de-inactivates. Experimental data is from a sharp electrode recording from an OT cell in the SON of the hypothalamic explant. Note that all spikes have been clipped for clarity.

4. Discussion

We have developed mathematical models of both species (OT and AVP) of SON magnocellular neurones. The models include many of the currents contributing to the regulation of their firing patterns, and reproduce a wide range of experimental protocols. While we have relied largely on published reports of electrical properties to parameterize our models, we have also presented new pharmacological data showing that a significant

component of the HAP is sustained by I_c. In addition we have presented new calcium imaging data that allows estimation of intracellular calcium transients controlling AHP's, HAP's and DAP's in these neurones.

4.1. Calcium Buffering and Calcium Dynamics

Our main experimental finding is the dissociation of time-scales between the rise and the clearance of somatic (bulk) calcium and the activation and de-activation of two of the three Ca^{2+}-activated K^+ channels that we have studied. We interpret this dissociation as implying strong calcium compartmentalization within the cell, which is possibly caused by calcium buffers. In fact Ca^{2+} buffering is known to be a crucial determinant of firing activity in these cells (Li et al., 1995). For example, the intrinsic buffers calretinin and calbindin-D_{28K} are localized to OT but not AVP neurones of the SON (Arai et al., 1996, 1999; Miyata et al., 1998). Recall that a key distinction between OT and AVP cells is the preferential ability of the latter to express a DAP. The presence or absence of these buffers modulates the DAP expression, since injection of calbindin-D_{28K} anti-serum unmasks the DAP and converts regularly firing cells to phasic cells. The converse is also true: injection of calbindin-D_{28K} into phasic cells suppresses the DAP and changes activity from phasic to continuous firing (Li et al., 1995).

4.2. Inhibitory Currents Regulating Excitability

In the normal rat, both OT and AVP cells emit a Poisson distributed *slow-irregular* ~1.5 Hz spike-train (Poulain et al., 1988). Each spike is caused by synaptically-driven random threshold crossings, and such firing patterns have been termed "occasional spiking" (Calvin, 1975). This discharge is tightly regulated by the inhibitory K^+ currents, I_c, I_{AHP}, I_A and I_{SOR}, and in fact MNC's will actively defend their intrinsic firing rate and compensate for evoked spikes by slowing their spontaneous discharge (Leng et al., 1995).

Our model shows that while each current plays a unique role in regulating firing, there are duplicate mechanisms for both short- and long-term inhibition in these cells that can be activated either by spike activity (I_c and I_{AHP}) or by modulations of the rest potential (I_A and I_{SOR}).

First I_c effects the post-spike refractory period *via* the HAP (Fig. 10), and so transiently lessens the cell's response to synaptic input. The function of the AHP is similar but it acts over a more sustained period (Fig. 9), and is only activated when two or more spikes are emitted proximally. Both of these currents therefore regulate discharge as a function of the cell's spiking history and maintain the variability of the spike train (Cazalis et al., 1985) by ensuring that short interspike-intervals tend to be followed by much longer intervals.

In contrast, the voltage-dependent currents I_A and I_{SOR} do not depend on prior activity but instead control excitability *via* the membrane potential. They are therefore more responsive to extraneous factors that manipulate the resting potential, such as synaptic input or neuromodulation, rather than intrinsic spike activity. The relative time-courses of I_A and I_{SOR} complement those of I_c and I_{AHP}: I_A recovers swiftly from inactivation and inactivates progressively during rapid firing, it therefore mediates short-term inhibition. On the other hand, I_{SOR} is slow and sustained and induces a long-term inhibition. Furthermore, these two currents are modulated by opposing stimuli: the removal of *A*-current inactivation (Fig. 7) is aggravated by longer hyperpolarizations, while I_{SOR} is activated by steady depolarizations (Fig. 13). Thus the excitability of OT cells (those that express I_{SOR}) is a bell shaped function of the holding potential (recall Fig. 13) while that of AVP cells (which do not express I_{SOR}) is an increasing function of the holding potential.

All four of these currents are targets for neuromodulators and can be up- or down-regulated during different physiological stresses. For example, during both pregnancy and lactation, the response of OT cells to other OT-releasing stimuli such as hyper-osmolality (Higuchi et al., 1988) is blunted. Coincidentally, the AHP (Teruyama and Armstrong, 2002) is up-regulated during this time and is likely to contribute to this diminished response. However, the decay of the AHP is also faster in OT neurons during lactation despite this increased amplitude, suggesting a complex scenario of state dependent AHP modulation. In addition, lactation induces an increase in the amplitude of the rebound-depolarization (RD) (Stern and Armstrong, 1996), but leaves the apparent SOR amplitude unaffected, suggesting a modulation of τ_{SOR} rather than the conductance. Alternatively, noting the strong interaction between I_A and the rebound depolarization, this could be caused by a change in the properties of I_A. All four currents can also be regulated indirectly, and can be tempered by activation of metabotropic glutamate receptors (mGluRs) (Schrader and Tasker, 1997). mGluR

up-regulation occurs during dehydration (Meeker et al., 1994) and probably further promotes cellular excitability during phasic firing.

4.3. The Osmotic Response

Although both hormones are released during hyperosmolality or dehydration, the two cell types respond differently to an increasing stress (Wakerley et al., 1978; Roper and Sherman, 2002). OT cells switch to a *fast-continuous* discharge that rarely exceeds 10 Hz, while AVP cells fire a phasic discharge pattern of lengthy repeating bursts, each of which rides upon a plateau potential (Andrew and Dudek, 1983). In Roper et al. (2003) we have shown that our model can also account for the plateau potential and for phasic activity.

The osmo-response in both cell types is mediated by a sustained depolarization of up to +15 mV, which has several contributing factors (see e.g. Voisin and Bourque, 2002). In our model for AVP cells, this net depolarization traverses the range of the voltage sensitivity of the DAP (Fig. 11), while for OT cells it traverses the activation of I_{SOR} (Fig. 13).

The plateau potential in phasic AVP cells is above spike threshold and is sustained by the regenerative summation of DAP's (see Fig. 14a). Thus, since dehydration increases DAP amplitude, it also facilitates phasic activity. However, although ∼30% of OT cells express a DAP (Armstrong et al., 1994), they rarely discharge phasically (Brimble and Dyball, 1977; Armstrong et al., 1994). Our model indicates that this disparity is due to the activation of I_{SOR} as the membrane potential approaches spike threshold. Therefore, although OT cells also exhibit DAP summation when concurrent spikes are evoked, I_{SOR} inhibits the cell and prevents it from spiking regeneratively. Summed DAP's then decay with their usual time-course (see Fig. 14c).

4.4. A Dual Role for Calcium

By activating the AHP, calcium is usually perceived as a messenger of electrical inhibition rather than excitation (see e.g. Vergara et al., 1998). However in AVP cells it plays two opposing roles: not only does it mediate both short- and long-term inhibition *via* the activation of BK and SK channels (I_c and I_{AHP}), but it can also excite the cell by turning off the resting K^+ current, $I_{K,\mathrm{leak}}$ (Li and Hatton, 1997b). Having two such antithetical functions

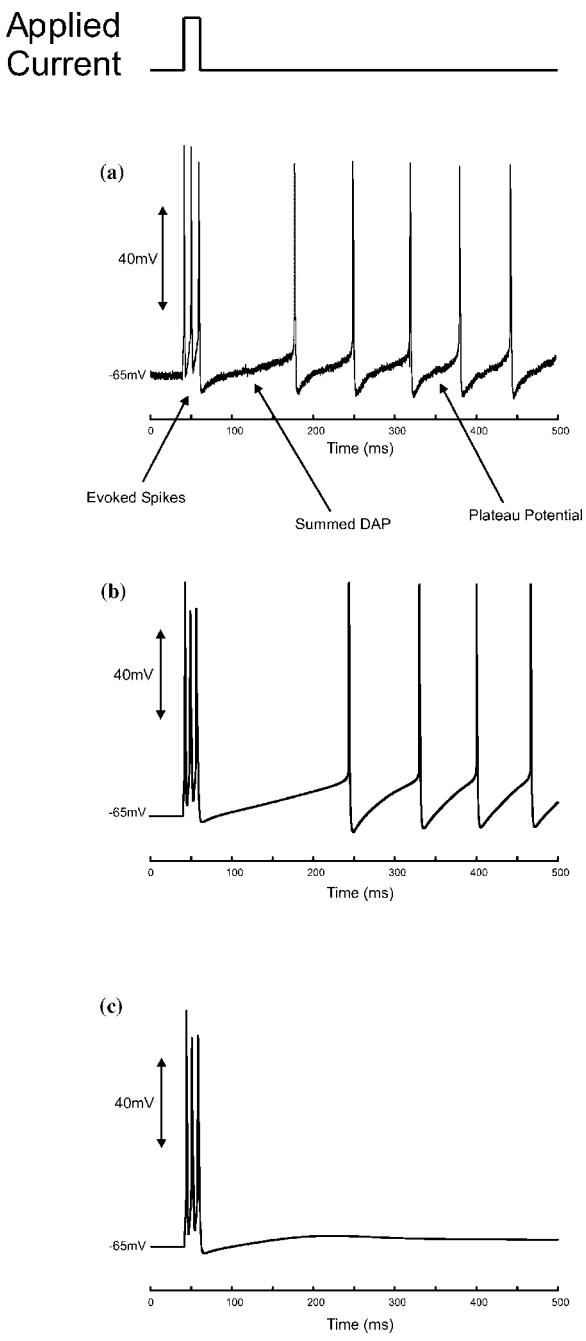

Figure 14. DAP summation and the initiation of phasic activity. (a) sharp electrode recording from SON of hypothalamic explant, (b) SON model with DAP, (c) SON model with DAP and SOR. (a) and (b): Three spikes are evoked by a short depolarizing pulse, and the subsequent DAP summation carries the membrane potential above spike threshold and causes a regenerative plateau potential. (c) The same model and protocol as (b) but with I_{SOR} included. The SOR inhibits the plateau and prevents regenerative firing, and the summed DAP decays to rest with the usual slow time course.

appears at first glance to be contradictory. However there is a delicate interplay between the DAP and the AHP that is dictated by their respective time-scales, and whether the cell exhibits a depolarizing or a hyperpolarizing after-potential depends both on the stimulation frequency and also the number of spikes in the train (Andrew and Dudek, 1984b). In phasic neurons strongly expressing DAP's, prolonged low frequency stimulation (<1 Hz) evokes single spikes and consequent DAP's, which then fade to the resting potential. At intermediate frequencies (>1 and <10 Hz) the DAP's sum to form a regenerative depolarized plateau potential which can then support endogenous firing *via* positive feedback (Andrew and Dudek, 1983). In contrast, at higher frequencies (>10 Hz) the AHP becomes predominant and instead a net hyperpolarization occurs (see Fig. 1b). Thus calcium acts here both to amplify signals of a certain bandwidth, and to filter stimulation that is of too high or too low a frequency. Furthermore, since the DAP is also voltage-dependent, this signal processing is labile and depends on the membrane potential. Thus dehydration magnifies the gain of the amplification, and contributes to the phasic activity seen in AVP cells under increased osmotic stress (Wakerley et al., 1978).

Appendix

The full model is given by

$$\frac{\mathrm{d}V}{\mathrm{d}t} = -\frac{1}{\mathcal{C}}(I_{\mathrm{Na}} + I_{\mathrm{Ca}} + I_K + I_A + I_c + I_{\mathrm{AHP}} + I_{\mathrm{SOR}} + I_{\mathrm{leak}})$$

and we have assumed the specific capacitance to be $\mathcal{C} = 1$.

Recall from Eq. (4) that inactivating and non-inactivating currents are respectively described by

$$I_\gamma = g_\gamma m^\alpha h^\beta (V - E_\gamma) \quad \text{or} \quad I_\gamma = g_\gamma m^\alpha (V - E_\gamma)$$

and their corresponding voltage-dependent activation (m_∞) and inactivation (h_∞) functions are

$$m_\infty(V) = \left(1 + \exp\left(\frac{-V - V_m}{k_m}\right)\right)^{-1} \quad \text{and}$$

$$h_\infty(V) = \left(1 + \exp\left(\frac{V + V_h}{k_h}\right)\right)^{-1}$$

Reversal potentials are $E_{\mathrm{Na}} = 50$ mV, $E_K = -96$ mV, $E_{\mathrm{Ca}} = 12.5 \ln([\mathrm{Ca}^{2+}]_o / [\mathrm{Ca}^{2+}]_i)$, and we have assumed the external calcium concentration to be $[\mathrm{Ca}^{2+}]_o = 4$ mM.

The parameters for each voltage-dependent current are tabulated below

	g_γ (mS cm^{-2})	V_m (mV)	k_m (mV)	V_h (mV)	k_h (mV)
$I_{\mathrm{Na}} = g_{\mathrm{Na}} m_\infty^3 h (V - E_{\mathrm{Na}})$	14	38	4	45	2
$I_{\mathrm{Ca}} = g_{\mathrm{Ca}} m_\infty^2 (V - E_{\mathrm{Ca}})$	0.1	−10	7	–	–
$I_{\mathrm{DR}} = g_{\mathrm{DR}} m^3 (V - E_K)$	14	−2	11	–	–
$I_{\mathrm{A}} = g_{\mathrm{A}} m^4 h (V - E_K)$	14	45	11	80	6.5
$I_{\mathrm{SOR}} = g_{\mathrm{SOR}} m (V - E_K)$	0.06	60	1.8	–	–
$I_{\mathrm{AHP}} = g_{\mathrm{AHP}} q_\infty^2 (V - E_K)$	0.18	–	–	–	–
$I_c = g_c p (V - E_K)$	1	–	–	–	–

and the corresponding time constants (in ms) for each current are

I_{Na}	τ_m	–
	τ_h	$\frac{20}{\left(1+\exp\left(\frac{V-1}{14}\right)\right)\left(1+\exp\left(\frac{V+30}{34}\right)\right)} - 0.075$
I_{Ca}	τ_m	$\left(0.19\left(\frac{-V+19.88}{\exp\left(\frac{-V+19.88}{10}-1\right)}\right) + 0.046\exp\left(\frac{-V}{20.73}\right)\right)^{-1}$
	τ_h	–
I_{DR}	τ_m	$\frac{8}{\exp\left(\frac{V+40}{19}\right)+\exp\left(\frac{-V-40}{20}\right)} + 1.8$
	τ_h	–
I_A	τ_m	$\frac{35}{1.1\exp\left(\frac{V+43}{17}\right)+\exp\left(\frac{-V-20}{13}\right)}$
	τ_h	$5 + \frac{120}{\exp\left(\frac{V+75}{30}\right)+\exp\left(\frac{-V-45}{18}\right)}$
I_{AHP}	τ_m	–
	τ_h	–
I_c	τ_m	1.22
	τ_h	–
I_{SOR}	τ_m	260
	τ_h	–

The calcium-dependent activation functions for I_{AHP} and I_c (respectively q and p) have been described previously in the text, but for completeness they are

$$q_\infty(C_{\mathrm{SK}}) = \left(1 + \exp\left[-1.120 - 2.508 \log\left(\frac{C_{\mathrm{SK}} - C_r}{1000}\right)\right]\right)^{-1}$$

$$p_\infty(C_{\mathrm{BK}}, V) = \left[1 + \frac{470}{C_{\mathrm{BK}}^{2.38}}\right]^{-1} \times \left[1 + \exp\left(\frac{(-V - 140\log_{10} C_{\mathrm{BK}} + 370)}{7.4}\right)\right]^{-1}$$

where C_{BK} denotes the calcium concentration in the pool sensed by the BK channel, C_{BK} denotes the concentration in the AHP calcium domain, and C_r (= 113 nM) the resting calcium concentration.

Each of the three calcium pools evolves according to (recall Eq. (8))

$$\frac{\mathrm{d}}{\mathrm{d}t}C_\gamma = -\alpha_\gamma I_{\mathrm{Ca}} - \frac{1}{\tau_\gamma}(C_\gamma - C_r)$$

with time constants $\tau_i = 2.33$ s (C_i), $\tau_{\mathrm{BK}} = 1$ ms (C_{BK}) and $\tau_{\mathrm{SK}} = 656$ ms (C_{SK}), and Faraday scaling factors $\alpha_i = 1.4$, $\alpha_{\mathrm{BK}} = 100$ and $\alpha_{\mathrm{SK}} = 1.6$.

The leak current is the linear sum of two distinct currents

$$I_{\mathrm{leak}} = I_{\mathrm{Na,leak}} + I_{K,\mathrm{leak}}$$

and $I_{K,\mathrm{leak}}$ can be modulated by both intra-cellular calcium and voltage according to

$$f_\infty(C_i, V) = \lambda - \Gamma a_\infty(C_i) b_\infty(V) \qquad (16)$$

where

$$a_\infty(C_i) = \tanh\left(\frac{C_i - C_r}{k_a}\right) \quad \text{and}$$
$$b_\infty(V) = \left[1 + \exp\left(-\frac{V + V_b}{k_b}\right)\right]^{-1} \qquad (17)$$

with $k_a = 50$ nM, $k_b = 8$ mV, $V_b = -60$ mV, the resting calcium concentration is $C_r = 113$ nM, and while b activates instantaneously, a evolves with $\tau_a = 75$ ms.

Acknowledgments

We would like to thank Arthur Sherman for guidance and support during the preparation of this work, and Bard Ermentrout for releasing, and supporting XP-Paut (http://www.math.pitt.edu/~bard/xpp/xpp.html), which was used for all of our numerical work. We would also like to thank David Brown, Gareth Leng and Françoise Moos for advice on an earlier version of this model, and Victor Matveev for a careful reading and critique of this manuscript.

This work was supported by an NIH IRTA Fellowship (PR) and by NIH grant numbers NS23941(WEA) and NS42276(JCC).

Note

1. In other preparations this after-potential is often termed the fast AHP (fAHP) (see e.g. Storm, 1987), but the term HAP is usual in the SON MNC literature (Bourque et al., 1985).

References

Adams PR, Constanti A, Brown DA, Clark RB (1982a) Intracellular Ca^{2+} activates a fast voltage-sensitive K^+ current in vertebrate sympathetic neurones. Nature, 296(April): 746–749.

Adams PR, Brown DA, Constanti A (1982b) M-currents and other potassium currents in bullfrog sympathetic neurons. Journal of Physiology (London) 330: 537–572.

Andrew RD (1987) Endogenous bursting by rat supraoptic neuroendocrine cells is calcium dependent. Journal of Physiology (London) 384: 451–465.

Andrew RD, Dudek FE (1983) Burst discharge in mammalian neuroendocrine cells involves an intrinsic regenerative mechanism. Science 221(4615): 1050–1052.

Andrew RD, Dudek FE (1984a) Analysis of intracellularly recorded phasic bursting by mammalian neuroendocrine cells. Journal of Neurophysiology 51(3): 552–566.

Andrew RD, Dudek FE (1984b) Intrinsic inhibition in magnocellular neuroendocrine cells of rat hypothalamus. Journal of Physiology (London) 353: 171–185.

Aradi I, Holmes WR (1999) Role of multiple calcium and calcium-dependent conductances in regulation of hippocampal dentate granule cell excitability. Journal of Computational Neuroscience 6: 215–235.

Arai R, Jacobowitz DM, Nagatsu I (1996) Calretinin is differentially localized in magnocellular oxytocin neurons of the rat hypothalamus. A double-labeling immunofluorescence study. Brain Research 735(1): 154–158.

Arai R, Jacobowitz DM, Hida T (1999) Calbindin D28k and calretinin in oxytocin and vasopressin neurons of the rat supraoptic nucleus: A triple-labeling immunofluorescence study. Cell and Tissue Research 298(1): 11–19.

Armstrong WE, Smith BN (1990) Tuberal supraoptic neurons II: Electrotonic properties. Neuroscience 38(2): 485–494.

Armstrong WE, Smith BN, Tian M (1994) Electrophysiological characteristics of immunochemically identified rat oxytocin and vasopressin neurons in vitro. Journal of Physiology (London) 475(1): 115–128.

Bains JS, Ferguson AV (1999) Activation of N-methyl-D-aspartate receptors evokes calcium spikes in the dendrites of rat hypothalamic paraventricular nucleus neurons. Neuroscience 90(3): 885–891.

Blackwell KT (2002) The effect of intensity and duration on the light-induced sodium and potassium currents in the *Hermissenda* type B photoreceptor. Journal of Neuroscience 22: 4217–4228.

Borg-Graham L (1987) Modelling the somatic electrical behavior of hippocampal pyramidal neurons. M.Phil. thesis, Massachusetts Institute of Technology, Department of Electrical Engineering and Computer Science. Also appears as MIT AI Lab TR 1161.

Borg-Graham LJ (1999) Interpretations of data and mechanisms for hippocampal pyramidal cell models. In: PS Ulinski, EG Jones, A Peters, eds. Models of Cortical Circuits. Cerebral Cortex, New York: Plenum Press, Vol. 13, Chap. 2, pp. 19–138 .

Bourque CW (1986) Calcium-dependent spike after-current induces burst firing in magnocellular neurosecretory-cells. Neuroscience Letters 70(2): 204–209.

Bourque CW (1988) Transient calcium-dependent potassium current in magnocellular neurosecretory cells of the rat supraoptic nucleus. Journal of Physiology (London) 397: 331–347.

Bourque CW, Brown DA (1987) Apamin and d-tubocurarine block the after-hyperpolarization of rat supraoptic neurosecretory neurons. Neuroscience Letters 82(2): 185–190.

Bourque, CW, Renaud LP (1988) Activity dependence of action potential duration in neurosecretory cells. In: G Leng ed. Pulsatility in Neuroendocrine Systems. CRC Press, Inc., Boca Raton, FL: Chap. 11, pp. 197–203.

Bourque CW, Randle JCR, Renaud LP (1985) Calcium-dependent potassium conductance in rat supraoptic nucleus neurosecretory neurons. Journal of Neurophysiology 54(6): 1375–1382.

Bourque CW, Kirkpatrick K, Jarvis CR (1998) Extrinsic modulation of spike afterpotentials in rat hypothalamoneurohypophysial neurons. Cellular and Molecular Neurobiology 18(1): 3–12.

Brimble MJ, Dyball REJ (1977) Characterization of oxytocin- and vasopressin-secreting neurones in the supraoptic nucleus to osmotic stimulation. Journal of Physiology (London) 271: 253–271.

Brown DA (2000) Neurobiology: The acid test for resting potassium channels. Current Biology 10: R456–R459.

Calvin WH (1975) Generation of spike trains in CNS neurons. Brain Research 84(1): 1–22.

Cazalis M, Dayanithi G, Nordmann JJ (1985) The role of patterned burst and interburst interval on the excitation-coupling mechanism in the isolated rat neural lobe. Journal of Physiology (London) 369: 45–60.

Chad JE, Eckert R (1984) Calcium domains associated with individual channels can account for anomalous voltage relations of Ca-dependent responses. Biophysical Journal 45(5): 993–999.

Cobbett P, Mason WT (1987) Whole cell voltage clamp recordings from cultured neurons of the supraoptic area of neonatal rat hypothalamus. Brain Research 409(1): 175–180.

Cobbett P, Legendre P, Mason WT (1989) Characterization of 3 types of potassium current in cultured neurons of rat supraoptic nucleus area. Journal of Physiology (London) 410: 443–462.

Dopico AM, Widmer H, Wang G, Lemos JR, Treistman SN (1999) Rat supraoptic magnocellular neurones show distinct large conductance, Ca^{2+}-activated K^+ channel subtypes in cell bodies versus nerve endings. Journal of Physiology (London) 519(1): 101–114.

Ermentrout B (2002) Simulating, Analyzing, and Animating Dynamical Systems: A Guide to XPPAUT for Researchers and Students. SIAM, Philadelphia, PA.

Fisher TE, Bourque CW (1995) Voltage-gated calcium currents in the magnocellular neurosecretory cells of the rat supraoptic nucleus. Journal of Physiology (London) 486(3): 571–580.

Fisher TE, Bourque CW (1998) Properties of the transient K^+ current in acutely isolated supraoptic neurons from adult rat. Advances in Experimental Medicine and Biology 449: 97–106.

Fisher TE, Voisin DL, Bourque CW (1998) Density of transient K^+ current influences excitability in acutely isolated vasopressin and oxytocin neurones of rat hypothalamus. Journal of Physiology (London) 511(2): 423–432.

Foehring RC, Armstrong WE (1996) Pharmacological dissection of high-voltage-activated Ca^{2+} current types in acutely dissociated rat supraoptic magnocellular neurons. Journal of Neurophysiology 76(2): 977–983.

Ghamari-Langroudi M, Bourque CW (2000) Excitatory role of the hyperpolarization-activated inward current in phasic and tonic firing of rat supraoptic neurons. Journal of Neuroscience 20: 4855–4863.

Ghamari-Langroudi M, Bourque CW (2002) Flufenamic acid blocks depolarizing afterpotentials and phasic firing in rat supraoptic neurones. Journal of Physiology (London) 545(2): 537–542.

Golowasch J, Goldman MS, Abbott LF, Marder E (2002) Failure of averaging in the construction of a conductance-based neuron model. Journal of Neurophysiology 87(2): 1129–1131.

Greene CC, Schwindt PC, Crill WE (1994) Properties and ionic mechanisms of a metabotropic glutamate receptor-mediated slow afterdepolarization in neocortical neurons. Journal of Neurophysiology 72(2): 693–704.

Greffrath W, Martin E, Reuss S, Boehmer G (1998) Components of after-hyperpolarization in magnocellular neurons of the rat supraoptic nucleus in vitro. Journal of Physiology (London) 513(2): 493–506.

Grynkiewicz G, Poenie M, Tsien RY (1985) A new generation of Ca^{2+} indicators with greatly improved fluorescence properties. Journal of Biological Chemistry 260(6): 3440–3450.

Han J, Gnatenco C, Sladek CD, Kim D (2003) Background and tandem-pore potassium channels in magnocellular neurosecretory cells of the rat supraoptic nucleus. Journal of Physiology 546: 625–639.

Higuchi T, Honda K, Takano S, Negoro H (1988) Role of the supraoptic nucleus in regulation of parturition and milk ejection revisited. Journal of Endocrinology 116(2): 225–230.

Hille B (2001) Ionic Channels of Excitable Membranes. Third edn. Sunderland, Massachusetts: Sinauer Associates Inc.

Jahromi BS, Zhang L, Carlen PL, Pennefather P (1999) Differential time-course of slow afterhyperpolarizations and associated Ca^{2+} transients in rat CA1 pyramidal neurons: further dissociation by Ca^{2+} buffer. Neuroscience 88(3): 719–726.

Joux N, Chevaleyre V, Alonso G, Boissin-Agasse L, Moos FC, Desarménien MG, Hussy N (2001) High voltage-activated Ca^{2+} currents in rat supraoptic neurones: biophysical properties and expression of the various channel $\alpha 1$ subunits. Journal of Neuroendocrinology 13(7): 638–649.

Kirkpatrick K (1997) Functional role and modulation of a calcium-activated potassium current in rat supraoptic neurons in vitro. Ph.D. thesis, Department of Neurology and Neurosurgery, McGill University, Montreal.

Kirkpatrick K, Bourque CW (1995) Effects of neurotensin on rat supraoptic nucleus neurons in vitro. Journal of Physiology (London) 482(2): 373–381.

Kirkpatrick K, Bourque CW (1996) Activity dependence and functional role of the apamin-sensitive K^+ current in rat supraoptic

neurones in vitro. Journal of Physiology (London) 494(2): 389–398.

Komori Y, Dayanithi G, Sasaki N, Ishii1 M, Ueta Y, Shibuya I (2001) Analysis of the Ca^{2+} clearance mechanism of rat supraoptic neurons. Society for Neuroscience Abstracts 27(178.2).

Lambert RC, Dayanithi G, Moos FC, Richard P (1994) A rise in the intracellular Ca^{2+} concentration of isolated rat supraoptic cells in response to oxytocin. Journal of Physiology (London) 478(2): 275–287.

Lancaster B (1991) Isolation of potassium currents. In: J Chad, H Wheal, eds. Cellular Neurobiology: A Practical Approach. Oxford University Press, New York, Chap. 6, pp. 97–119 .

Lancaster B, Zucker RS (1994) Photolytic manipulation of Ca^{2+} and the time-course of slow, Ca^{2+}-activated K^+ current in rat hippocampal-neurons. Journal of Physiology (London) 475: 229–239.

Lasser-Ross N, Miyakawa H, Lev-Ram V, Young SR, Ross WN (1991) High time resolution fluorescence imaging with a CCD camera. Journal of Neuroscience Methods 36(2/3): 253–261.

Lasser-Ross N, Ross WN, Yarom Y (1997) Activity-dependent $[Ca^{2+}]_i$ changes in guinea pig vagal motoneurons: Relationship to the slow afterhyperpolarization. Journal of Neurophysiology 78(2): 825–834.

Leng G, Brown D, Murphy NP (1995) Patterning of electrical activity in magnocellular neurones. In: T Saito, K Kurokawa, S Yoshida, eds. Neurohypophysis, Recent Progress of Vasopressin and Oxytocin Research. Proceedings of the 1st Joint World Congress of Neurohypophysis and Vasopressin, Nasu, Tochigi, Japan. Elsevier Science B.V., Amsterdam, pp. 225–235.

Li ZH, Hatton GI (1997a) Ca^{2+} release from internal stores: Role in generating depolarizing after-potentials in rat supraoptic neurones. Journal of Physiology (London) 498(2): 339–350.

Li ZH, Hatton GI (1997b) Reduced outward K^+ conductances generate depolarizing after-potentials in rat supraoptic nucleus neurones. Journal of Physiology (London) 505(1): 95–106.

Li ZH, Decavel C, Hatton GI (1995) Calbindin-D_{28k}—role in determining intrinsically generated firing patterns in rat supraoptic neurons. Journal of Physiology (London) 488(3): 601–608.

Luther JA, Tasker JG (2000) Voltage-gated currents distinguish parvocellular from magnocellular neurones in the rat hypothalamic paraventricular nucleus. Journal of Physiology (London) 523(1): 193–209.

McCormick DA, Huguenard JR (1992) A model of the electrophysiological properties of thalamocortical relay neurons. Journal of Neurophysiology 68(4): 1384–1400.

Meeker RB, McGinnis S, Greenwood RS, Hayward JN (1994) Increased hypothalamic glutamate receptors induced by water deprivation. Neuroendocrinology 60(5): 477–485.

Miyata S, Khan AM, Hatton GI (1998) Colocalization of calretinin and calbindin-D_{28k} with oxytocin and vasopressin in rat supraoptic nucleus neurons: A quantitative study. Brain Research 785(1): 178–182.

Nagatomo T, Inenaga K, Yamashita H (1995) Transient outward current in adult-rat supraoptic neurons with slice patch-clamp technique: Inhibition by angiotensin-II. Journal of Physiology (London) 485(1): 87–96.

North RA (2000) Potassium-channel closure taken to TASK. Trends in Neurosciences 23(6): 234–235.

Oliet SHR, Bourque CW (1992) Properties of supraoptic magnocellular neurons isolated from the adult-rat. Journal of Physiology (London) 455: 291–306.

Plant RE (1978) The effects of calcium++ on bursting neurons: A modeling study. Biophysical Journal 21: 217–237.

Poulain DA, Brown D, Wakerley JB (1988) Statistical analysis of patterns of electrical activity in vasopressin- and oxytocin-secreting neurones. In: G Leng ed., Pulsatility in Neuroendocrine Systems. Boca Raton, Florida: CRC Press, Inc, Chap. 8, pp. 119–154.

Reid G, Flonta ML (2001) Cold transduction by inhibition of a background potassium conductance in rat primary sensory neurones. Neuroscience Letters 297: 171–174.

Roper P, Callaway JC, Armstrong WE (2001) Reconstructing phasic vasopressin cells. Society for Neuroscience Abstracts 27(178.3).

Roper P, Sherman A (2002) Mathematical analysis of firing pattern transitions in rat son magnocellular neurosecretory cells subject to osmotic stress. Society for Neuroscience Abstracts 28(273.3).

Roper P, Callaway J, Armstrong W (2003) Burst Initiation and Termination in Phasic Vasopressin Cells of the Rat SON: A Combined Mathematical, Electrical and Calcium Fluorescence Study. The Journal of Neuroscience, Submitted.

Sah P (1992) Role of calcium influx and buffering in the kinetics of a Ca^{2+}- activated K^+ current in rat vagal motoneurons. Journal of Neurophysiology 68(6): 2237–2247.

Schrader LA, Tasker JG (1997) Modulation of multiple potassium currents by metabotropic glutamate receptors in neurons of the hypothalamic supraoptic nucleus. Journal of Neurophysiology 78(6): 3428–3437.

Selyanko AA, Sim JA (1998) Ca^{2+}-inhibited non-inactivating K^+ channels in cultured rat hippocampal pyramidal neurones. Journal of Physiology (London) 510(1): 71–91.

Shao LR, Halvorsrud R, Borg-Graham L, Storm JF (1999) The role of BK-type Ca^{2+}-dependent K^+ channels in spike broadening during repetitive firing in rat hippocampal pyramidal cells. Journal of Physiology (London) 521(1): 135–146.

Simon SM, Llinas RR (1985) Compartmentalization of the submembrane calcium activity during calcium influx and its significance in transmitter release. Biophysical Journal 48(3): 485–498.

Stern JE, Armstrong WE (1995) Electrophysiological differences between oxytocin and vasopressin neurons recorded from female rats in vitro. Journal of Physiology (London) 488(3): 701–708.

Stern JE, Armstrong WE (1996) Changes in the electrical properties of supraoptic nucleus oxytocin and vasopressin neurons during lactation. Journal of Neuroscience 16(16): 4861–4871.

Stern JE, Armstrong WE (1997) Sustained outward rectification of oxytocinergic neurones in the rat supraoptic nucleus: Ionic dependence and pharmacology. Journal of Physiology (London) 500(2): 497–508.

Stern JE, Galarreta M, Foehring RC, Hestrin S, Armstrong WE (1999) Differences in the properties of ionotropic glutamate synaptic currents in oxytocin and vasopressin neuroendocrine neurons. Journal of Neuroscience 19(9): 3367–3375.

Storm JF (1987) Action-potential repolarization and a fast after-hyperpolarization in rat hippocampal pyramidal cells. Journal of Physiology (London) 385: 733–759.

Storm JF (1993) Functional diversity of K^+ currents in hippocampal pyramidal neurons. Seminars in the Neurosciences 5: 79–92.

Teruyama R, Armstrong WE (2002) Changes in the active membrane properties of rat supraoptic neurons during pregnancy and lactation. Journal of Neuroendocrinology 14: 1–17.

Van Goor F, Li YX, Stojilkovic SS (2001) Paradoxical role of large-conductance calcium-activated K^+ (BK) channels in controlling action potential-driven Ca^{2+} entry in anterior pituitary cells. Journal of Neuroscience 21: 5902–5915.

Vergara C, Latorre R, Marrion, NV, Adelman JP 1998. Calcium-activated potassium channels. Current Opinion in Neurobiology 8(3): 321–329.

Voisin DL, Bourque CW (2002) Integration of sodium and osmosensory signals in vasopressin neurons. Trends in Neurosciences 25(4): 199–205.

Wakerley JB, Lincoln DW (1973) The milk-ejection reflex of the rat: A 20- to 40-fold acceleration in the firing of paraventricular neurones during oxytocin release. Journal of Endocrinology 57: 477–493.

Wakerley JB, Poulain DA, Brown D (1978) Comparison of firing patterns in oxytocin- and vasopressin-releasing neurones during progressive dehydration. Brain Research 148: 425–440.

Warman EN, Durand DM, Yuen GLF (1994) Reconstruction of hippocampal CA1 pyramidal cell electrophysiology by computer-simulation. Journal of Neurophysiology 71: 2033–2045.

Wilson CJ, Callaway JC (2000) Coupled oscillator model of the dopaminergic neuron of the substantia nigra. Journal of Neurophysiology 83(5): 3084–3100.

Yuen GLF, Durand D (1991) Reconstruction of hippocampal granule cell electrophysiology by computer-simulation. Neuroscience 41(2/3): 411–423.